N O T I C E

THIS DOCUMENT HAS BEEN REPRODUCED FROM MICROFICHE. ALTHOUGH IT IS RECOGNIZED THAT CERTAIN PORTIONS ARE ILLEGIBLE, IT IS BEING RELEASED IN THE INTEREST OF MAKING AVAILABLE AS MUCH INFORMATION AS POSSIBLE

CR-166234

ASRL TR 196-2

ALLEVIATION OF HELICOPTER FUSELAGE-INDUCED ROTOR UNSTEADY LOADS THROUGH DETERMINISTIC VARIATION OF THE INDIVIDUAL BLADE PITCH

by

Mohammad A. Rahnema

May 1981

Prepared under Research Grant No. NSG-2266 by

Aeroelastic and Structures Research Laboratory
Department of Aeronautics and Astronautics
Massachusetts Institute of Technology
Cambridge, Massachusetts 02139

for

AMES RESEARCH CENTER
NATIONAL AERONAUTICS AND SPACE ADMINISTRATION
MOFFETT FIELD, CALIFORNIA 94035

ALLEVIATION OF HELICOPTER FUSELAGE-INDUCED ROTOR UNSTEADY LOADS THROUGH DETERMINISTIC VARIATION OF THE INDIVIDUAL BLADE PITCH

by

MOHAMMAD A. RAHNEMA

ABSTRACT

The effect of fuselage-induced upwash on the flapwise motion of a hinged rotor blade is considered. The typical upwash field is simulated through the flow produced by a moving point source. The resulting blade response is then approximated by its rigid flapping and first bending mode. The perturbation blade pitch variation required to alleviate its response to the upwash in the sense of either reducing the increased hub shear or minimization of the blade overall time averaged deflection, is determined. Calculations are carried out for a model rotor and for the case with increased Lock number. The results are presented in graphical form and are discussed in Chapter 5. It is found that the minimum blade deflection criteria suppress the rigid flapping by a large amount and reduce the peak-to-peak value of the blade hub shear by at least 50% without causing an additional increase in blade stresses.

Supervisor: Dr. Norman D. Ham

Title: Professor of Aeronautics and Astronautics

TABLE OF CONTENTS

PARTIAL LIST OF SYMBOLS

a	Blade section lift coefficient, per radian
c	Blade chord length
c_R	Blade aspect ratio (c/R)
d	Largest diameter of simulated fuselage
e	Blade hinge offset
$g(t)$	Displacement of blade first elastic bending mode
h	Height of rotor plane above the fuselage axis
ℓ	Distance of rotor axis from the fuselage nose
$m(r)$	Blade spanwise mass distribution
r	Spanwise distance along blade from its axis of rotation
R	Blade rpm (rotor radius)
$T(r)$	Blade section aerodynamic list, per unit span
X	Blade nondimensional blade spanwise coordinate (r/R)
X_A	Chordwise distance of section aerodynamic center from elastic axis
z	Blade flapwise deflection
$\beta(t)$	Displacement of blade rigid flapping mode
γ	Blade mass constant, Loch number
$\eta(r)$	Modal shape of blade first elastic bending mode
$\eta_k(r)$	Modal shape of blade kth bending mode
μ	Rotor advance ratio ($V_\infty/\Omega R$)
ν_k	Nondimensional rotating blade natural frequency of kth bending mode
Ω	Rotor angular velocity (radian/sec)

ψ	Rotor blade azimuth angle, zero when blade is downstream
ρ	Air density
θ	Blade pitch angle (positive, leading edge up)
ξ	Nondimensional blade hinge offset (e/R)
λ	Fuselage upwash flow (V/V_∞)

CHAPTER 1

INTRODUCTION

Earlier investigations have shown that the flow disturbances due to the fuselage of a helicopter result in an increase of the unsteady loads and motion experienced by the rotor. In an experiment conducted by Scheiman [1] it was found that the predicted blade loadings for an S58 helicopter were appreciably different from the measured values over a narrow band of azimuth angles centered on 180°. The discrepancy was found to be resolved through a modification of the blade incidence in a manner that was consistent with the upwash flow provided by the fuselage. Since then further studies have led to the conclusion that the influence of the fuselage can be significant on the rotor blade loading [2]. Such an interference effect is likely to be enhanced in the case of the more compact design of modern helicopters in which the clearance between the fuselage and rotor is reduced.

The unsteady aerodynamic perturbation forces arising from the passage of the blade through the fuselage upwash flow leads to significant blade and hub vibratory response in a manner depending on the aeroelastic properties of the blades. The occurrence of stall phenomena is alsc a possibility caused by the increased blade incidence. This produces a considerable variation in blade drag leading to an increase in the blade bending and in-plane hub forces. The increase in the blade torsional moment is then reflected in an oscillation imposed on the control loads.

Such considerations from both the aerodynamic and the structural point of view would justify any attempt toward the development of a method

for the alleviation of the undesirable effects of the fuselage induced upwash on the rotor. A simple technique to offset the upwash flow (in cases where raising of the rotor height is not desirable) would be an automatic variation of the blade pitch as it enters the region of fuselage disturbance. In this way the effective blade incidence is decreased and is thus a useful means in situations where stall might be predominant. However, observation of the flow field of a typical helicopter fuselage shows that the effect of the upwash flow on the blade incidence can not be totally offset through a spanwise uniform reduction in the blade pitch. As may be seen from Fig. (2.3a) the fuselage upwash does not vary linearly over the blade span but varies in a rather parabolic fashion from the hub to the tip with its maximum somewhere near the middle of the blade span. Therefore, even with a pitch reduction, the spanwise non-uniformity left in the blade loading due to the fuselage will excite the flapwise bending modes of the blade generating inertia forces which couple with the aerodynamic forces and makes the vibration alleviation aspect of the problem more subtle through simple blade pitch control.

It is speculated that the second flap mode may be the dominant excited bending mode as it is most similar in shape to the form of the spanwise non-uniformity of the forcing load (i.e. upwash flow). This expectation turns out to be consistent with the result of certain experimental observations [2]. Since, the frequency of the 2nd flap mode in a full scale helicopter is about 3 per rotor revolution, any blade pitch control for alleviation of the vibratory forces and motion of the rotor would have to be effected through approximately the same frequency. Control

of rotor blades at these vibratory frequencies has become a possibility through the introduction of the multicyclic or Higher Harmonic Control (HHC). The individual-blade-control (IBC) concept is a version of the HHC approach in which signals from sensors mounted on the blades are used to supply appropriate control commands to the broad-band electrohydraulic actuators attached to the individual blade. The (IBC) concept has been investigated by serveral researchers in its applicability to gust and vibration alleviation systems. The interested reader is encouraged to consult the listed references [3-5].

However, since the means for higher harmonic control of blade pitch have already been devised and are currently under further investigation, the question to be asked in this thesis is what time variation of the individual blade pitch would best suppress the vibratory forces and motions of the rotor caused by the aerodynamic interference of the fuselage. It is, of cource, being assumed that the deterministic approach (open loop) to the pitch control would be the best choice in this case as both the form and the location of any disturbance due to fuselage is fixed. Besides, in a feed back control loop, any sensor mounted on the blade would sense any random disturbance that might occur and thus the control of a well specified regular disturbance is made more complicated. In Chapter Two, the upwash flow of a simple hull-shaped body is calculated which will be used as the approximately simulated upwash of a practical fuselage. A simplified version of the flutter equation as derived in [6] are used in Chapter Three tc calculate the hinged blade flapwise response equations for the perturbation forces caused by the fuselage disturbance and the

control pitch input. The blade flapwise motion is approximated by the rigid-flapping and the first bending modes. The criteria used in later chapters for the calculation of the control blade pitch input are either the reduction of the perturbation axial hub shear or the minimization of the overall time-averaged deflection of the blade caused by the fuselage effect. The rigid and first bending modes with the thus-obtained control pitch input are individually calculated and are shown in each case. The numerical calculations are carried out for both a model and a full scale rotor and the effect of the increase of rotor advance ratio is studied.

It is hoped that the trends in the control pitch data obtained here will be helpful in any future (IBC) design for alleviation of the fuselage-induced rotor stresses and vibration.

CHAPTER 2

SIMULATION OF FUSELAGE UPWASH FIELD

In practical helicopters, the shape of the fuselage varies from one type to another and each produces a different disturbance to the upcoming flow. The upwash component of the disturbance at the plane of the rotor, which contributes most to a change of blade incidence angle, has been calculated for a number of different fuselages and is reported in [2]. The common characteristics evident from the results of those calculations are a variation of the upwash at 180° azimuth angle from a peak value between .1 and .15 of free stream velocity at 40% of rotor radius to a negligibly small value at the rotor tip. The results also show a rather rapid decrease of the peak value of upwash with azimuth angle such that the value at 40% rotor radius drops to half its maximum value (at 180° azimuth) over 25 degrees to 30 degrees of azimuth.

These features will here be approximately simulated through combination of the flow field of a single source with that of a parallel flow. In this way, we will be able to derive rather simple analytical expressions for the upwash flow.

Consider one three-dimensional source with a volume flow intensity of I_0 so that the induced velocity is $I_0/4\pi r_0^2$, where r_0 denotes the distance from the source. By superposing a flow of constant and parallel velocity V (the forward flight velocity) to this source, a flow field like that shown in Fig. (2.1) is resulted. The flow field, as illustrated in the figure, is divided into two parts by one streamline (which splits into branches to

all sides in three-dimensional space) and divides the flow supplied by the source from the parallel flow. This streamline goes through the stagnation point A whose distance from the source point may be calculated by consider- that the source velocity there is neutralized by the parallel flow, that is

$$V - \frac{I_o}{4\pi r_o^2} = 0$$

and thus

$$r_{o_A} = \sqrt{\frac{I_o}{4\pi V}}$$

The source intensity may be expressed in terms of the maximum diameter of the stream surface of revolution through the stagnation point. This is done by considering that at infinite distance from the source, the fluid supply I_0 provided by the source should equal the amount of parallel flow that would have passed through the cross section $\pi \frac{d^2}{4}$, that is

$$I_o = \pi \frac{d^2}{4} V$$

To compute the shape of the stream surface with the maximum diameter d, let the point source be the origin of a system of polar coordinates ρ_0, ψ. Then on any point on the streamline through point A (see Fig. 2.1), we can write

$$\frac{d\rho_o}{\rho_o d\varphi} = \frac{V_{\rho_o}}{V_\varphi}$$

$$= \frac{V \sin\varphi + I_o/4\pi\rho_o^2}{-V \sin\varphi}$$

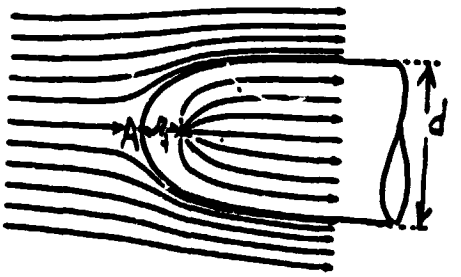

FIG. 2.1a Superposition of Point Source with Parallel Flow

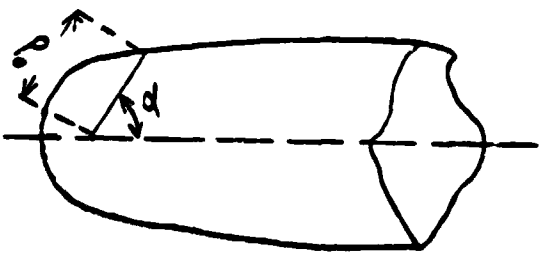

FIG. 2.1b Representation of Coordinates Referring to Fuselage Shape

which gives

$$\frac{d\rho_0}{d\varphi} = -\rho_0 \cot\varphi - \frac{I_0}{4\pi V \sin\varphi}$$

and has to satisfy the condition

$$\rho_0 = r_{0_A} \quad \text{at} \quad \varphi = 180^\circ$$

the solution is found to be

$$\rho_0 = \frac{d}{4\sin\frac{\varphi}{2}} \tag{2.1}$$

after incorporating the expressions for I_0 and r_A in the equation.

Equation (2.1) gives the shape of the axisymmetric body that when placed in the parallel flow would produce the same flow field that the source would do in the space outside the body. The upwash produced when moved parallel to its axis is simply the vertical component of the source velocity. With the rotor placed at a height h above the body axis (Fig. 2.2), simple considerations of the geometry and the source velocity (given by $\pi d^2 V/16 r_0^2$) will show that the upwash flow in the plane of the rotor is given by:

$$\frac{V_{up}}{V} = \frac{h d^2}{16\left[h^2 + \left(\ell - \frac{d}{4}\right)^2 + \lambda^2 - 2\lambda\left(\ell - \frac{d}{4}\right)\cos(\pi - \psi)\right]^{3/2}} \tag{2.2}$$

where ℓ is the distance of the body nose from the rotor hub axis.

The values of the various parameters in (2.2) that were used to generate the upwash are given below:

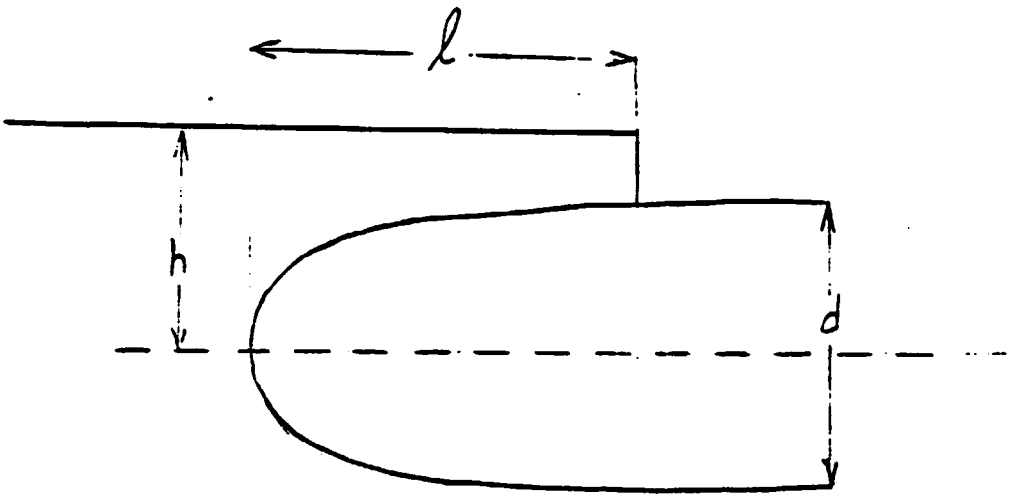

FIG. 2.2 Rotor-Fuselage Orientation

$h = 4.75"$

$\ell = 13.94"$

$d = 6"$

and $R = 24.38"$ (same as the radius of the MIT (IBC) model rotor).

With the above values, Equation (2.2) becomes

$$k \equiv \frac{V_{up}}{V} = \frac{.79}{16\left[4.92 + 16.52\left(\frac{r}{R}\right)^2 - 16.86\left(\frac{r}{R}\right)\sin(\pi - \psi)\right]^{3/2}} \qquad (2.2a)$$

The function is displayed graphically in Figs. (2.3). In Fig. (2.3a) the radial variation of the simulated upwash at 180° azimuth is shown and Fig. (2.3b) gives its peak value (at about 50% rotor radius) against azimuth angle.

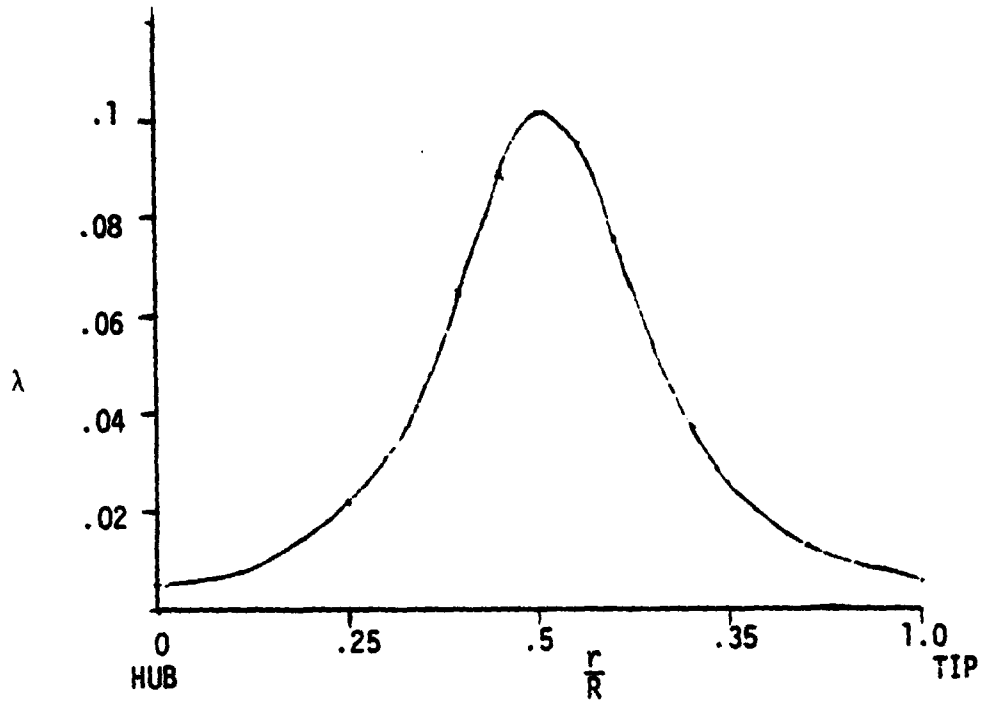

(a) Radial Variation of the Upwash at 180° Azimuth

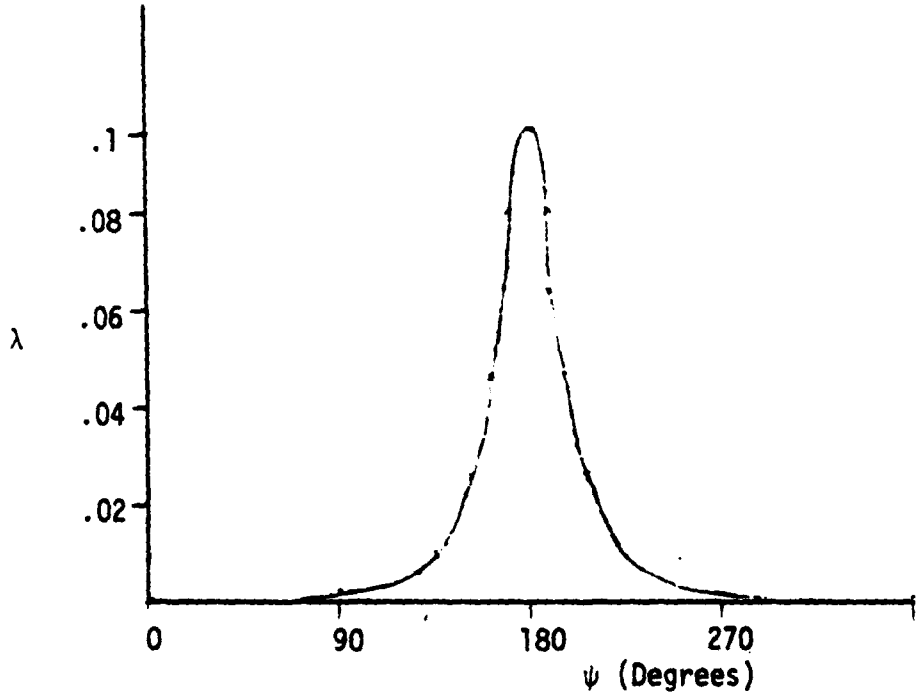

(b) Azimuth Variation of the Peak Value (at about 50% Radius)

FIG. 2.3 Fuselage Upwash Generated from Eq. (2.2a)

CHAPTER 3

BLADE DYNAMIC RESPONSE

This chapter presents the aeroelastic equations governing blade flapwise motion. The flapping motion is expected to be the one most influenced by the upwash effect of the fuselage which causes an increase in the blade section lift. It will be assumed that the elastic axis of the blade passes through the center of gravity at any section along the span so that the bending motion is decoupled from any torsional or pitch motion of blade due to control loads. The more general case combining blade torsion and bending is treated in [6]. The bending equation is derived for a hinged blade with generally a hinge offset (e) and the rigid flap and first bending modes are used to approximate blade deflection. The modal equation thus obtained are seen to have periodic time varying coefficients caused through the chaning flow direction "seen" by the blade in forward flight. The equations are then simplified by using the periodic coefficients in a time averaged sense. This may be justified through the assumption that the time varying part of the coefficients are small relative to thei: mean values, which happen to be the case for low values of advance ratio. The solutions obtained using the time averaged equations can then be assumed to be slightly different from those obtained from the exact equations through a small oscillatory perturbation.

The procedure followed here is basically the same as detailed in [6]. The bending moment at r due to forces at S for the rotating blade deflected out of the plane of rotation (Fig. 3.1) is

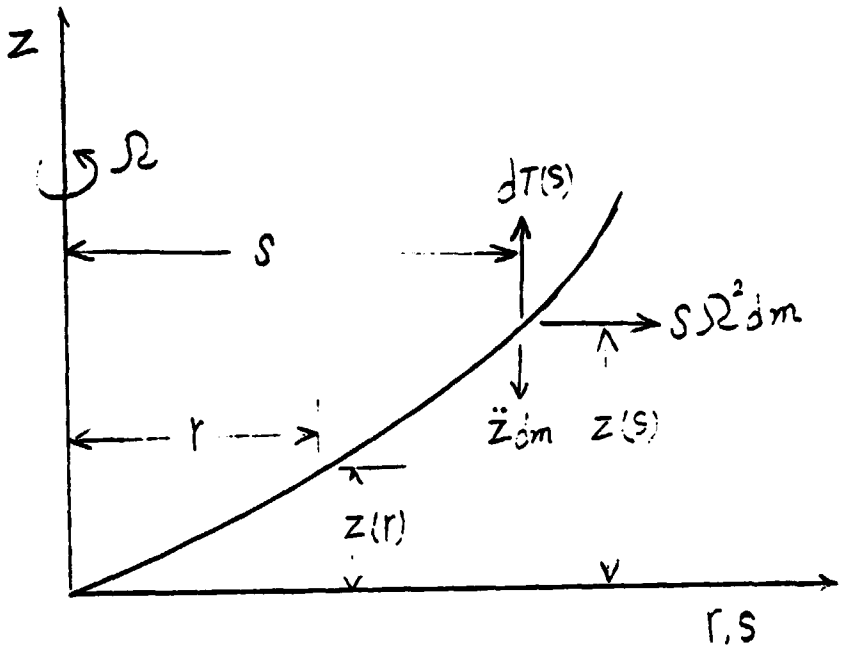

FIG. 3.1 Blade Bending Geometry

$$M(r) = \int_r^R \left[\frac{dT(s)}{ds} - \ddot{z}(s)m(s)\right](s-r)ds - \int_r^R g\Omega^2 m(s)[z(s)-z(r)]ds$$

From simple beam theory, the bending moment is related to the beam elasticity through

$$M(r) = EI(r)\frac{d^2z}{dr^2}$$

which upon substituting in the expression for the bending moment and differentiating twice with respect to r gives

$$\frac{d^2}{dr^2}\left[EI(r)\frac{d^2z}{dr^2} - \frac{d^2z}{dr^2}\right] - \frac{d^2z}{dr^2}\int_r^R m(s)g\Omega^2 ds + r\Omega^2 m(r)\frac{dz}{dr} + m(r)\ddot{z} = \frac{dT}{dr} \tag{3.1}$$

The solution to Equation (3.1) may be expressed as the sum of the normal bending modes weighted by some time dependent functions $g_k(t)$ to be found,

$$Z(r,t) = \sum_{K=1}^{\infty} \eta_K(r)\, g_K(t)$$

Substituting in Eq. (3.1) leads to

$$\sum_{K=1}^{\infty}\left\{\left[\frac{d^2}{dr^2}\left(EI\frac{d^2\eta_K}{dr^2}\right) - \frac{d^2\eta_K}{dr^2}\int_r^R m(s)g\Omega^2 ds + r\,m(r)\Omega^2\frac{d\eta_K}{dr}\right]g_K + m\eta_K\ddot{g}_K\right\} = 0 \tag{3.1a}$$

For free vibration of the rotating beam without aerodynamic forcing ($\frac{dT}{dr} = 0$) the $g_k(t)$ may be assumed to be simple harmonic function of the form

$$q_K(t) = \bar{q}_K e^{i\nu_K \Omega t}$$

where ν_k is the kth rotating undamped natural frequency of the blade.

With this, Eq. (3.1a) becomes

$$\sum_{K=1}^{\infty} \left\{ [\quad] q_K - m \eta_K \nu_K^2 \Omega^2 q_K \right\} = 0$$

Since this equation should hold for all feasible values of r at any time t, the logical consequence is

$$[\quad] - m \eta_K \nu_K^2 \Omega^2 = 0 \tag{3.2}$$

Equation (3.2) is then the condition that the normal bending modes have to satisfy.

The bending equation of motion (3.1a) then is simplified to

$$\sum_{K=1}^{\infty} m \nu_K^2 \Omega^2 \eta_K q_K + \sum_{K=1}^{\infty} m \eta_K \ddot{q}_K = \frac{dT}{d\Omega} \tag{3.1b}$$

Multiplying both sides of Eq. (3.1b) by η_k and integrating from 0 to R with regard to orthogonality of the $\eta_{k's}$ give

$$M_K \ddot{q}_K + M_K \nu_K^2 \Omega^2 q_K = \int_0^R \eta_K \frac{dT}{d\Omega} d\Omega \tag{3.3}$$

where

$$M_K \equiv \int_0^R m \eta_K^2 d\Omega$$

Approximating the deflection of the hinged blade by the rigid flap and first bending mode

$$z = (r-e)\beta(t) + r\, g(t) \tag{3.4}$$

where e is generally some hinge offset and $\beta \equiv g_1$, $g \equiv g_2$. Equation (3.3) then gives the following modal equations

$$\frac{\ddot{\beta}}{\Omega^2} + \nu_1^2 \beta = \frac{1}{M_1 \Omega^2} \int_e^R (r-e) \frac{dT}{dr} dr \tag{3.5}$$

$$\frac{M_2}{M_1} \frac{\ddot{g}}{\Omega^2} + \frac{M_2}{M_1} \nu_2^2 g = \frac{1}{M_1 \Omega^2} \int_e^R r \frac{dT}{dr} dr \tag{3.6}$$

The aerodynamic lift term (dT/dr) is from unsteady theory for thin airfoil oscillating in incompressible flow

$$\frac{dT}{dr} = -\frac{1}{8}\rho a c^2 \left[\ddot{z} - U_T \dot{\theta} + (x_A - .25c)\ddot{\theta}\right]$$
$$-\frac{1}{2}\rho a c U_T C'(K)\left[U_P - U_T\theta - (.5c - x_A)\dot{\theta}\right] \tag{3.7}$$

in which the unsteady effects due to variation of the blade transverse velocity (U_T) is neglected, and $C'(K)$ is the equivalent of the Theodorson

function C(K) for rotors. For quasi-steady airflow $C'(K) = 1$, which will be used here.

The blade transverse (U_T) and perpendicular velocity relative to air mass are respectively

$$U_T = \Omega r + \mu \Omega R \sin\psi$$

$$U_p = \dot{z} + \mu \Omega R \frac{dz}{dr} \cos\psi - \mu \Omega R \lambda \tag{3.8}$$

where λ is the fuselage upwash given by Eq. (2.2a).

The virtual mass terms proportional to $\ddot{z}$ and $\ddot{\theta}$ in Eq. (3.3) will be neglected here. However, their small contribution (of the order of a few percent) could be included through appropriate adjustment of blade inertia constants.

Then, with the expression for $\frac{dT}{dr}$ given in Eq. (3.5), the modal Eqs. (3.5, 3.6) take the form

$$\beta'' + m_{\beta_1}\beta' + m_{g_1}g' + m_{\beta_1}\beta + m_{g_1}g = m_{\theta_1'}\theta' + m_{\theta_1}\theta + F_{\lambda_1}(\psi) \tag{3.9a}$$

$$g'' + m_{\beta_2'}\beta' + m_{g_2'}g' + m_{\beta_2}\beta + m_{g_2}g = m_{\theta_2'}\theta' + m_{\theta_2}\theta + F_{\lambda_2}(\psi) \tag{3.9b}$$

where the primes denote differentiation with respect to time and we used ($\frac{d}{dt} = \Omega \frac{d}{d\psi}$). Note that $\psi = \Omega t$. The expression for the various coefficients m_β', m_g', ... and the upwash forcing functions $F_{\lambda_1}(\psi)$, $F_{\lambda_2}(\psi)$ are given in Appendix A, and B.

Using a hinge offset of $\frac{e}{R} = .0821$ (the value for the MIT IBC rotor) and an approximate function for the bending mode given by $\frac{\eta}{R} = 4(\frac{x-\xi}{1-\xi})^2 - 3(\frac{x-\xi}{1-\xi})$; ($\xi \equiv \frac{e}{R}$). The coefficients in Eqs. (3.9) in <u>time averaged form</u> become:

$$m_{\beta_1}' = .118\gamma \qquad m_{\beta_2}' = .0208\gamma\frac{M_1}{M_2}$$

$$m_{g_1}' = .0208\gamma \qquad m_{g_2}' = .0568\gamma\frac{M_1}{M_2}$$

$$m_{\beta_1} = \nu_1^2 \qquad m_{\beta_2} = 0$$

$$m_{g_1} = 0 \qquad m_{g_2} = \nu_2^2$$

$$m_{\theta_1}' = .119\gamma(\frac{c}{R}) \qquad m_{\theta_2}' = -.00469\gamma(\frac{c}{R})$$

$$m_{\theta_1} = .121\gamma + .115\mu^2\gamma \qquad m_{\theta_2} = (.0188 - .0382\mu^2)\gamma\cdot\frac{M_1}{M_2}$$

(3.10)

It is to be noted that the values for m_{θ_1} and m_{θ_2} are valid for $x_A = 0$ (blade section aerodynamic center on elastic axis of blade) which is nearly true for the MIT IBC rotor blade. Otherwise they would have to be recalculated using the equations in Appendix A.

The ratio $\frac{M_1}{M_2}$ is given by

$$\frac{M_1}{M_2} = \frac{\int_\xi^1 m\left(\frac{x-\xi}{1-\xi}\right)^2 dx}{\int_\xi^1 m\left(\frac{\eta}{R}\right)^2 dx} \qquad (3.11)$$

For uniform blade mass distribution, RM = 1.666.

The coupled modal differential equations expressed in Eq. (3.9) give the hinged blade bending response to the blade pitch angle (θ) and the fuselage upwash effect represented by the (F) functions. By setting θ equal to zero in the linear equations, the bending contribution from the fuselage upwash is obtained. However, the solution to Eqs. (3.9) for any given variation of the pitch angle θ and the F functions with the approximate time averaged constant coefficients given in Eq. (3.10) may be constructed through simply a superposition of the individual harmonic solutions which can easily be obtained. To express the nth harmonic component of the solution in terms of that of the forcing terms, let

$$\theta(\psi) = \theta_n^c \cos n\psi + \theta_n^s \sin n\psi$$

$$F_{\lambda_1}(\psi) = F_{\lambda_{1n}}^c \cos n\psi + F_{\lambda_{2n}}^s \sin n\psi$$

$$F_{\lambda_2}(\psi) = F_{\lambda_{2n}}^c \cos n\psi + F_{\lambda_{2n}}^s \sin n\psi$$

and assume a response of the form

$$\beta(\psi) = \beta_n^c \cos n\psi + \beta_n^s \sin n\psi$$

$$g(\psi) = g_n^c \cos n\psi + g_n^s \sin n\psi$$

Substituting these in Eqs. (3.9) and equating the coefficients of cos $n\psi$ and sin $n\psi$ on both sides of each equation, leads to the following

four equations expressed in matrix form for the unknown β_n^c, β_n^s, g_n^c and g_n^s.

$$\underset{\sim}{[C]}\left\{\underset{\sim}{D}\right\} = \underset{\sim}{[R]}\begin{Bmatrix}\theta_n^c\\ \theta_n^s\end{Bmatrix} + \left\{\underset{\sim}{F}\right\} \tag{3.12}$$

where

$$\underset{\sim}{[C]} = \begin{bmatrix} -.118n\gamma & -n^2+v_1^2 & -.0208n\gamma & 0 \\ -n^2+v_1^2 & .118n\gamma & 0 & .0208n\gamma \\ -.0208\gamma(RM)n & 0 & -.0568\gamma(RM)n & -n^2+v_2^2 \\ 0 & .0208\gamma(RM)n & -n^2+v_2^2 & .0568\gamma(RM)n \end{bmatrix}$$

$$\underset{\sim}{[R]} = \begin{bmatrix} -.119n\gamma(CR) & (.121+.115\mu^2)\gamma \\ (.121+.115\mu^2)\gamma & .119n\gamma(CR) \\ .00469n\gamma(CR) & (.0188-.0382\mu^2)\gamma(RM) \\ (.0188-.0382\mu^2)\gamma(RM) & -.00469n\gamma(CR) \end{bmatrix}$$

and

$$\left\{\underset{\sim}{F}\right\} = \begin{Bmatrix} F_{\lambda_1 n}^s \\ F_{\lambda_1 n}^c \\ F_{\lambda_2 n}^s \\ F_{\lambda_2 n}^c \end{Bmatrix}, \quad \left\{\underset{\sim}{D}\right\} = \begin{Bmatrix} \beta_n^c \\ \beta_n^s \\ g_n^c \\ g_n^s \end{Bmatrix} \tag{3.13}$$

In the next chapter, the control pitch requirement for reduction of fuselage-induced blade hub shear will be determined. The minimization of the blade deflection is also considered. The equations involved are solved through harmonic superposition using the modal equations in the form of Eq. (3.11).

CHAPTER 4

PITCH CONTROL ALLEVIATION OF THE FUSELAGE INDUCED ROTOR STRESS AND VIBRATION

The blade flapwise motion contributed by the periodic lift effect of the fuselage upwash flow localized around 180° azimuth adds to rotor vibratory motion. The lift increment coupled with the inertia reaction of the resulting blade motion produces unsteady shear forces at the blade root which may then cause a decrease in its fatigue life. It is thus noticed that the control of rotor response to the aerodynamic disturbance of fuselage, when significant, is important both from the vibration viewpoint and structurally. The blade vibratory motion may be controlled to some extent through variation of its pitch angle as is seen from the dynamic equation given in Eq. (3.9). It is then possible to determine the control pitch input that would reduce some of the undesirable effects of the fuselage disturbance. In the present chapter, the perturbation pitch angle required for reduction of blade axial hub shear is determined first and then in Section 4.2 the condition for minimization of blade deflection is considered.

4.1 Reduction of Increase Blade Hub Shear

The blade hub shear is obtained from integration of the lift and inertia forces along the span,

$$Sh = \int_e^R \frac{dT}{dr} dr - \int_e^R \ddot{z}\, dm \qquad (4.1.1)$$

From Eqs. (3.5) and (3.8) neglecting the terms involving $\ddot{z}$ and $\ddot{\theta}$,

$$\frac{dT}{d\Omega} \simeq \left[\frac{1}{8}\rho a c^2 + \frac{1}{2}\rho a c\, C'(K)(.5c - X_A)\right](\Omega R + \mu \Omega R \sin\psi)\dot{\theta}$$

$$+ \frac{1}{2}\rho a c\, C'(K)(\Omega R + \mu \Omega R \sin\psi)^2 \theta$$

$$- \frac{1}{2}\rho a c\, C'(K)(\Omega R + \mu \Omega R \sin\psi)\left(\dot{z} + \mu \Omega R \frac{dz}{d\Omega}\sin\psi - \mu \Omega R h\right)$$

where h is given in Eq. (2.2), and

$$z = \eta_1 \beta + \eta_2 g$$

$$= R\left\{\left(\frac{x-\varepsilon}{1-\varepsilon}\right)\beta + \left[4\left(\frac{x-\varepsilon}{1-\varepsilon}\right)^2 - 3\left(\frac{x-\varepsilon}{1-\varepsilon}\right)\right] g\right\}$$

assuming quasi-steady airflow, $C'(K) = 1$, and for a zero value of X_A, and $\frac{e}{R} = .082$, the expression for shear (4.1.1) is integrated into

$$Sh = -\frac{1}{2}\rho a c R^3 \left\{-\mu \int_\varepsilon^1 h x\, dx - (\mu^2 \sin\psi)\int_\varepsilon^1 h\, dx\right.$$

$$+ (.318 + .459\mu \sin\psi)\beta' - (.011 + .153\mu \sin\psi) g'$$

$$+ (.541\mu \sin\psi + \tfrac{1}{2}\mu^2 \sin 2\psi)\beta + (1.153\mu \sin\psi + \tfrac{1}{2}\mu^2 \sin 2\psi) g$$

$$+ \frac{2}{\gamma}(X_1 \beta'' + X_2 g'') - \frac{1}{3}\left[(1 + 1.38\mu^2) + 2.75\mu \sin\psi - 1.38\mu \sin 2\psi\right]\theta$$

$$\left. - \left[.355(cR) + .69(cR)\mu \sin\psi\right]\theta' \right\}$$

(4.1.2)

where

$$X_1 \equiv \frac{\int_e^R \left(\frac{n_1}{R}\right) m(\ell)\, d\ell}{\int_e^R (n_1/R)^2 m(\ell)\, d\ell} \qquad (4.1a)$$

$$X_2 \equiv -\frac{\int_e^R \left(\frac{n_2}{R}\right) m(\ell)\, d\ell}{\int_e^R (n_1/R)^2 m(\ell)\, d\ell}$$

For uniform blade mass distribution; $X_1 = 1.5$, $X_2 = -.5$.

Using the time averaged form of the coefficient involving harmonic terms, Equation (4.1.2) is approximated to

$$Sh \simeq -\tfrac{1}{2}\rho a c R^3 \left[-\mu \int_1^1 \lambda x\, dx + .318\beta' - .011 g' - \tfrac{1}{3}(1+1.38\mu^2)\theta \right.$$

$$\left. - .355(cR)\theta' + \frac{2}{\gamma}\left(X_1 \beta'' + X_2 g''\right)\right]$$

(4.1.2a)

The function $\theta(\psi)$ is now to be determined in such a way that the shear is reduced to a fraction S, $(0 < S \leq 1)$ of its value without control pitch input. That is,

$$Sh = S \cdot (Sh)_{\theta=0}$$

which on using Eq. (4.1.2a) gives

$$-(1-S)\mu T(\psi)+.318(\theta'-S\underline{\beta}')-.011(\underline{g}'-S\underline{g}')+\frac{2}{\gamma}[X_1(\underline{\beta}''-S\underline{\beta}'')$$
$$+X_2(\underline{g}''-S\underline{g}'')]-\frac{1}{3}(1+1.38\mu^2)\theta-.375(CR)\theta'=0$$

where
$$T(\psi)\equiv\int_{\Sigma}^{1}\lambda x\,dx \tag{4.1.3}$$

is given in integrated form in Appendix B. While $\underline{\beta}$ and $\underline{g}$ are to be obtained from the modal Equation (3.9) with θ set to zero. They simply represent the blade response to fuselage upwash, alone (with no control pitch input).

Substituting the Fourier expansion of θ, β and g in the form

$$\theta(\psi)=\theta_0+\sum_n(\theta_n^c\cos n\psi+\theta_n^s\sin n\psi)$$
$$\beta(\psi)=\beta_0+\sum_n(\beta_n^c\cos n\psi+\beta_n^s\sin n\psi)$$
$$g(\psi)=g_0+\sum_n(g_n^c\cos n\psi+g_n^s\sin n\psi) \tag{4.1.4}$$

with similar expressions for $\underline{\beta}$ and $\underline{g}$ into Eq. (4.1.3) and equating the coefficients of cos $n\psi$ and sin $n\psi$ and the constant term to zero leads to the following equations.

$$\theta_0=\frac{-3(1-S)\mu T_0}{1+1.38\mu^2} \tag{4.1.5}$$

$$[\underset{\sim}{P}]\begin{Bmatrix}\theta_m^c\\ \theta_m^s\end{Bmatrix}=[\underset{\sim}{\Psi}]\left[\{\underset{\sim}{D}\}-S\{\underline{\underline{D}}\}\right]-\mu(1-S)\begin{Bmatrix}\tau_m^c\\ \tau_m^s\end{Bmatrix} \tag{4.1.6}$$

where

$$[\underset{\sim}{P}]=\begin{bmatrix}\frac{1}{3}(1+1.38\mu^2), & .375(cR)n\\ -.375(cR)n, & \frac{1}{3}(1+1.38\mu^2)\end{bmatrix} \tag{4.1.7}$$

$$[\underset{\sim}{\Psi}]=\begin{bmatrix}-\frac{2}{\gamma}X_1n^2, & .318n, & -\frac{2}{\gamma}X_2n^2, & -.011n\\ -.318n, & -\frac{2}{\gamma}X_1n^2, & .011n, & -\frac{2}{\gamma}X_2n^2\end{bmatrix}$$

and $\{\underset{\sim}{D}\}$ is calculated from Eq. (3.12) with $\{\theta\}$ set to zero,

$$\{\underset{\sim}{D}\}=[\underset{\sim}{C}]^{-1}\{\underset{\sim}{F}\} \tag{4.1.8}$$

From modal Equation, 3.12, can express $\{\underset{\sim}{D}\}$ in terms of $\{\theta\}$

$$\{\underset{\sim}{D}\}=[\underset{\sim}{C}]^{-1}\left[[\underset{\sim}{R}]\begin{Bmatrix}\theta_m^c\\ \theta_m^s\end{Bmatrix}+\{\underset{\sim}{F}\}\right] \tag{4.1.9}$$

Place this into Eq. (4.1.6) and solve for $\begin{Bmatrix} \theta_n^c \\ \theta_n^s \end{Bmatrix}$

$$\begin{Bmatrix} \theta_n^c \\ \theta_n^s \end{Bmatrix} = \left[[P] - [Q][C]^{-1}[R] \right]^{-1} (1-S) \left[[Q][C]^{-1} \{F\} - \mu(1-S) \begin{Bmatrix} \tau_n^c \\ \tau_n^s \end{Bmatrix} \right] \tag{4.1.10}$$

which together with Eq. (4.1.5) allows the calculation of all the Fourier coefficients in the series expansion of θ, Eq. (4.1.4). The pitch angle thus obtained is expected to reduce the fuselage caused blade hub shear by (1-S) percent. The resulting blade response may then be calculated from Eq. (4.1.9). The constant β_0 and g_0 involved in the Fourier series of (Eq. (4.1.4) are obtained from Eqs. (3.9)

$$\beta_0 = \frac{\gamma(.121 + .115\mu^2)\theta_0 + F_{\lambda_0}}{\nu_1^2}$$

$$g_0 = \frac{\gamma(RM)(.0188 - .0382\mu^2)\theta_0 + F_{\lambda_{20}}}{\nu_2^2} \tag{4.1.11}$$

4.2 Minimum Time Averaged Blade Deflection

The blade flapping motion is an important factor in the noise generated by rotating blades. It is also considered that a major component of blade lagging motion (in-plane motion) is caused through the

coriolis effects associated with rotating blade moving out of its plane of rotation. However, it is possible, at least in principle, to minimize the overall time averaged blade deflection due to fuselage disturbance through appropriate pitch input.

The goal is to minimize the integral

$$I \equiv \int_0^{2\pi} \int_e^R z^2 \, d\bar{r} \, d\psi$$

with z given by:

$$z = R\left\{\left(\frac{\bar{r}-e}{1-e}\right)\beta(\psi) + \left[4\left(\frac{\bar{r}-e}{1-e}\right)^2 - 3\left(\frac{\bar{r}-e}{1-e}\right)\right] g(\psi)\right\}$$

Substituting in the integral and integrating from $\bar{r}$ = .0821 (hinge offset) to 1 gives

$$I = R(1-e)\int_0^{2\pi} \left(\frac{1}{3}\beta^2(\psi) + .2\, g^2(\psi)\right) d\psi \qquad (4.2.1)$$

with β and g governed by the dynamic equations expressed in Eqs. (3.9). The pitch θ that would minimize I is to be determined. This is a variational problem which will be solved here through harmonic expansion of the functions involved.

Let

$$\begin{aligned}
\beta(\psi) &= \beta_0 + \sum_n \left(\beta_n^c \cos n\psi + \beta_n^s \sin n\psi\right) \\
g(\psi) &= g_0 + \sum_n \left(g_n^c \cos n\psi + g_n^s \sin n\psi\right) \\
\theta(\psi) &= \theta_0 + \sum_n \left(\theta_n^c \cos n\psi + \theta_n^s \sin n\psi\right)
\end{aligned} \qquad (4.2.2)$$

Substituting in Eq. (4.2.1) and considering that

$$\int_0^{2\pi} \cos n\psi \sin m\psi \, d\psi = 0$$

$$\int_0^{2\pi} \cos^2 n\psi \, d\psi = \int_0^{2\pi} \sin^2 n\psi \, d\psi = \pi$$

I becomes

$$I = \pi R^2 (1-\xi)\left[\frac{2}{3}\theta_0^2 + \frac{1}{3}\sum_n (\theta_n^{c2} + \theta_n^{s2}) + .4 g_0^2 + .2 \sum_n (g_n^{c2} + g_n^{s2})\right] \tag{4.2.3}$$

in which the β_n and g_n'S are related to θ_n^c and θ_n^s through the dynamic equation expressed in harmonic form in Eq. (3.12),

$$\{\underset{\sim}{D}\} \equiv \begin{Bmatrix} \beta_n^c \\ \beta_n^s \\ g_n^c \\ g_n^s \end{Bmatrix} = [\underset{\sim}{C}]^{-1}[\underset{\sim}{R}] \begin{Bmatrix} \theta_n^c \\ \theta_n^s \end{Bmatrix} + [\underset{\sim}{C}]^{-1}\{\underset{\sim}{F}\} \tag{4.2.4}$$

Let for simplicity

$$[\underset{\sim}{C}]^{-1}[\underset{\sim}{R}] \equiv [\underset{\sim}{Z}]$$

The constants β_0 and g_0 are related to θ_0 through Eqs. (3.9),

$$\beta_0 = \frac{\gamma(.121+.115\mu^2)\theta_0 + F\lambda_{1_0}}{V_1^2}$$

$$g_0 = \frac{\gamma(RM)(.0188-.0382\mu^2)+F\lambda_{2_0}}{V_2^2} \qquad (4.2.5)$$

The minimum conditions for I are

$$\frac{\partial I}{\partial \theta_0} = 0$$

$$\frac{\partial I}{\partial \theta_n^c} = \frac{\partial I}{\partial \theta_n^s} = 0 \quad , \quad n = 1, 2, \cdots$$

which, using the expression for I from Eq. (4.2.3) leads to the following equation for θ_0 and the $\theta_n^{'s}$

$$\frac{1}{3}\beta_0 \frac{\partial \beta_0}{\partial \theta_0} + .2\, g_0 \frac{\partial g_0}{\partial \theta_0} = 0 \qquad (a)$$

$$\frac{1}{3}\left(\beta_n^c \frac{\partial \beta_n^c}{\partial \theta_n^c} + \beta_n^s \frac{\partial \beta_n^s}{\partial \theta_n^c}\right) + .2\left(g_n^c \frac{\partial g_n^c}{\partial \theta_n^c} + g_n^s \frac{\partial g_n^s}{\partial \theta_n^c}\right) = 0 \qquad (b)$$

$$\frac{1}{3}\left(\theta_m^c \frac{\partial \theta_m^c}{\partial \theta_m^s} + \theta_m^s \frac{\partial \theta_m^s}{\partial \theta_m^s}\right) + .2\left(g_m^c \frac{\partial g_m^c}{\partial \theta_m^s} + g_m^s \frac{\partial g_m^s}{\partial \theta_m^s}\right) = 0 \qquad (c)$$

From Eq. (4.2.5) and (a), θ_0 is found to be

$$\theta_0 = \frac{\dfrac{-F_{\lambda_{1_0}}(.121+.115\mu^2)}{v_1^4} - \dfrac{F_{\lambda_{2_0}}(.0188-.0382\mu^2)(.6)}{v_2^4}}{\dfrac{\gamma(.121+.115\mu^2)^2}{v_1^4} + \dfrac{\gamma(RM)^2(.0188-.0382\mu^2)^2(.6)}{v_2^4}} \qquad (4.2.6)$$

From (b) and (c) combined with Eq. (4.2.4) get

$$\left[\tfrac{1}{3}Z_{11}, \tfrac{1}{3}Z_{21}, .2Z_{31}, .2Z_{41}\right]\{D\} = 0$$

$$\left[\tfrac{1}{3}Z_{12}, \tfrac{1}{3}Z_{22}, .2Z_{32}, .2Z_{42}\right]\{D\} = 0$$

replacing $\{D\}$ by $\begin{Bmatrix}\theta_n^c \\ \theta_n^s\end{Bmatrix}$ through (4.2.4) leads to

$$\left[\tfrac{1}{3}Z_{11}, \tfrac{1}{3}Z_{21}, .2Z_{31}, .2Z_{41}\right]\left\{[Z]\begin{Bmatrix}\theta_m^c \\ \theta_m^s\end{Bmatrix} + [C]^{-1}\{F\}\right\} = 0 \qquad (b^1)$$

$$\left[\tfrac{1}{3}Z_{12}, \tfrac{1}{3}Z_{22}, .2Z_{32}, .2Z_{41}\right]\left\{[Z]\begin{Bmatrix}\theta_m^c \\ \theta_m^s\end{Bmatrix} + [C]^{-1}\{F\}\right\} = 0 \qquad (c^1)$$

Let for simplicity denote

$$[\underset{\sim}{O}] = \begin{bmatrix} \frac{1}{3}Z_{11}^2 + \frac{1}{3}Z_{21}^2 + .2Z_{31}^2 + .2Z_{41}^2 , & \frac{1}{3}Z_{11}Z_{12} + \frac{1}{3}Z_{21}Z_{22} + .2Z_{31}Z_{32} + .2Z_{41}Z_{42} \\ \frac{1}{3}Z_{11}Z_{12} + \frac{1}{3}Z_{21}Z_{22} + .2Z_{31}Z_{32} + .2Z_{41}Z_{42} , & \frac{1}{3}Z_{12}^2 + \frac{1}{3}Z_{22}^2 + .2Z_{32}^2 + .2Z_{42}^2 \end{bmatrix}$$

$$V = [\tfrac{1}{3}Z_{11}, \tfrac{1}{3}Z_{21}, .2Z_{31}, .2Z_{41}][\underset{\sim}{C}]^{-1}\{\underset{\sim}{F}\}$$

$$W = [\tfrac{1}{3}Z_{12}, \tfrac{1}{3}Z_{22}, .2Z_{32}, .2Z_{42}][\underset{\sim}{C}]^{-1}\{\underset{\sim}{F}\} \qquad (4.2.7)$$

Equation (b') and (c') then take the form

$$[\underset{\sim}{O}]\begin{Bmatrix} \theta_m^c \\ \theta_m^s \end{Bmatrix} = \begin{Bmatrix} -V \\ -W \end{Bmatrix}$$

giving

$$\begin{Bmatrix} \theta_m^c \\ \theta_m^s \end{Bmatrix} = [\underset{\sim}{O}]^{-1}\begin{Bmatrix} -V \\ -W \end{Bmatrix} \qquad (4.2.8)$$

The values of θ_0, θ_n^c and θ_n^s, S obtained from Eqs. (4.2.6, 8) are then used to calculate the required control pitch angle from its series expansions given in Eq. (4.2.2). The resulting blade response is subsequently obtained using Eqs. (4.2.5, 4) and the relation $Z = \eta_1 \beta + \eta_2 g$.

CHAPTER 5

NUMERICAL RESULTS AND DISCUSSION

Numerical calculations were carried out on a digital-analogue computer for the MIT (IBC) model rotor at values of advance ratio of .2 and .4. Figures 5.1-8 display the results graphically. The non-dimensional parameters characteristic of the rotor are summarized in Table 5.1. In order to study the full scale effects due to more effective flexibility of blade, numerical results were also obtained with a Lock number three times larger than its value for the model rotor and are shown in Figs. 5.9-16.

It is seen from Figures 5.1-16 that the required blade pitch variation for either reduced hub shear or minimum deflection of the blade barely exceeds a maximum of one degree in all cases. However, the extent to which the fuselage upwash as generated from Eq. (2.2a) would modify the effective blade section incidence may be calculated from the relation

$$\Delta\alpha = \mu \frac{h(x,\psi)}{x} \tag{5.1}$$

which turns out to give an average value of about +1 degree over the blade span at $\mu = .2$, and +2 degrees at $\mu = .4$; when the blade is at 180° azimuth, while the maximum pitch variation required for minimum overall blade deflection is seen from Figs. 5.4,8,12,16 to be about 0.3 and 0.7 degrees (for 180° azimuth position) at rotor advance ratios of .2 and .4, respectively. These figures are about one-third of the average change in incidence over the blade length as effected through the upwash flow. But, it is to be

noted from consideration of Eq. (5.1) or its plot in Fig. 5.0 that a much larger amount of the upwash induced blade incidence is concentrated over the inboard half of the rotor blade where not only the dynamic pressure is lower due to the small value of blade transverse velocity (Ωr), but also the contribution of the upwash loading to blade deflection is less because of the existence of a smaller moment arm over the inboard region of the blade.

The reduction of blade hub shear is seen to lead to an increase in the peak-to-peak variation of the bending mode (g), in general. Thus, the hub shear is alleviated at the expense of increasing blade bending stresses. One would then expect that in the full size rotor with more effective blade flexibility, the blade hub shear to be less than its value in the model rotor; which is found to be the case from comparison of Figs. 5.1,5,9,13. However, the increase in the bending mode peak-to-peak variation is seen from Figs. 5.1-16 to be by factors of about 1.6 and 2.4 for 80% and 100% reduced hub shear at $\mu = .2$, respectively. While, at rotor advance ratio of .4, the increase is seen to be by a factor of about 1.6 for both 80% and 100% (zero) reduction in blade hub shear. This indicates that it is possible to further reduce the blade hub shear at higher values of rotor advance ratio without causing additional increase in the blade bending stresses.

The blade rigid flapping is seen to be suppressed by a factor of about 7 through pitch control for zero hub shear. The figures show that the flapping (β) is generally decreased through hub shear reduction, which is not undesirable. Anyhow, the case in which the blade rigid flapping is

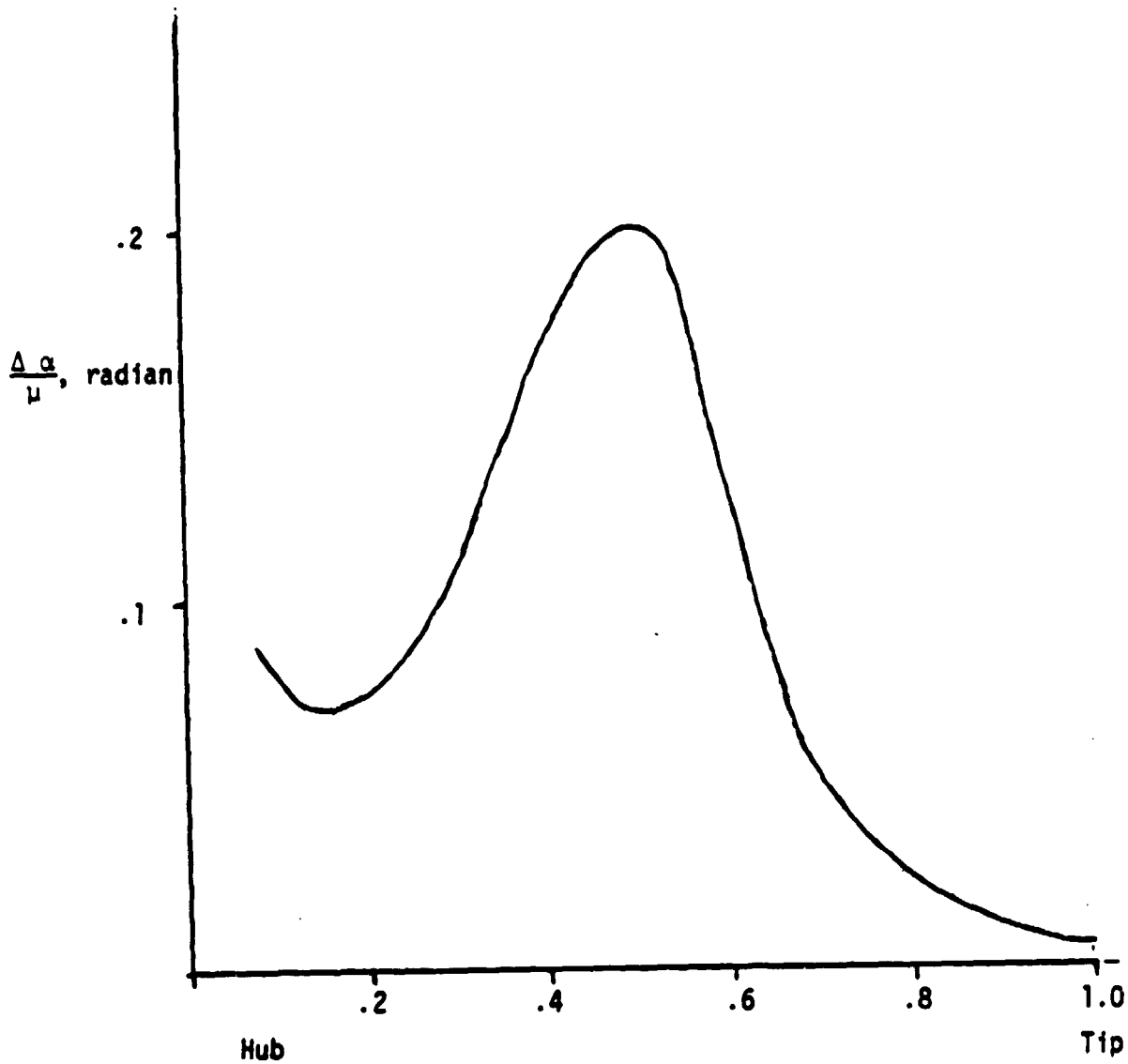

FIG. 5.0 Change in Blade Section Incidence Due to the Fuselage Upwash

suppressed best is seen to be that of the minimum deflection criteria. Figures 5.4,8,12,16 show a decrease in β by a factor of more than 70 with pitch variation for minimum blade deflection. The effect on the blade bending mode, in this case, is seen to be insignificant. The justification for this may be that the blade overall deflection, proportional to $(\beta^2 + .6g^2)$. is dominated by the value of β through the fact that it is an order of magnitude larger than g as seen from Figs. 5.1,5,9,13. However, the results do show a decrease in the hub shear by a factor from 4 to 5, but with increased oscillation.

The criteria of minimum blade deflections seem to be superior to that of shear reduction, except for causing increased oscillation in the blade hub shear. As, it suppresses the flapping mode by a large amount and reduces the hub shear by 70 to 80 per cent, while causing no increase in the bending mode, thus preventing additional blade stresses as a result of the control pitch input. Besides, it is observed from Figs. 5.4,8,12,16 that the pitch variation required in this case is easier to implement technically in contrast to the reduced shear condition which would require multi-cyclic variation of blade pitch 5.2,3,6,7.

TABLE 5.1

The values of the MIT (IBC) model rotor parameters as studied in the present work are listed below:

$\gamma = 2.294$

$\nu_1 = 1.078$

$\nu_2 = 3.55$ (at $\Omega = 12.5$ Hz)

$RM = (\equiv \frac{M1}{M2}) = .959$

$X_1 = 1.642$

$X_2 = -.661$ Defined in (4.1a)

$CR = .0821$

$\xi = .0821$

REFERENCES

1. Scheiman, J., "A Tabulation of Helicopter Rotor Blade Differential Pressures, Stresses, and Motions as Measured in Flight", NASA TMX-952, 1964.

2. Wilby, P.G., Young, C. and Grant, J., "An Investigation of the Fuselage Flow Field on Rotor Loads and the Effects of Vehicle Configuration", Vertica, Vol. 3, No. 2.

3. Ham, Norman D., "A Simple System for Helicopter Individual-Blade-Control Using Modal Decomposition", Vertica, Vol. 4, No. 1, 1980, pp. 23-28.

4. Shaw, J. and Albion, N., "Active Control of Rotor Blade Pitch for Vibration Reduction - A Wind Tunnel Demonstration", Vertica, Vol. 4, No. 1, 1980, pp. 3-11.

5. McKillip, Robert M., "The Design, Testing and Evaluation of the M.I.T. Individual-Blade-Control System as Applied to Gust Alleviation for Helicopters", MIT Aeroelastic and Structures Research Laboratory TR-196-1, February 1980.

6. Ham, Norman D., "Helicopter Blade Flutter", AGARD Report No. 607, 1973.

7. Gradshteyn, I.S. and Ryzhik, I.M., Table of Integrals, Series, and Products, Academic Press, New York and London, 1965.

8. Ralston, A., Mathematical Methods for Digital Computer, John Wiley & Sons, Inc., 1960.

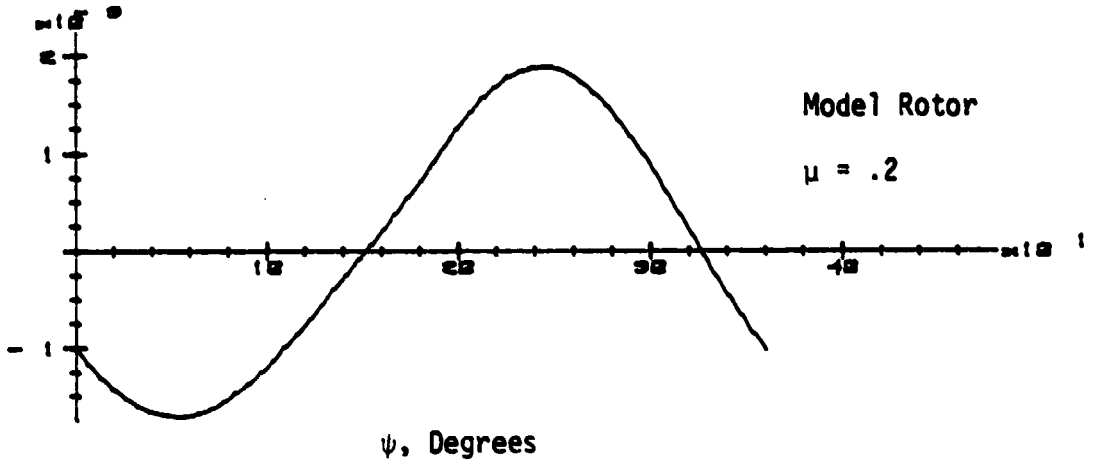

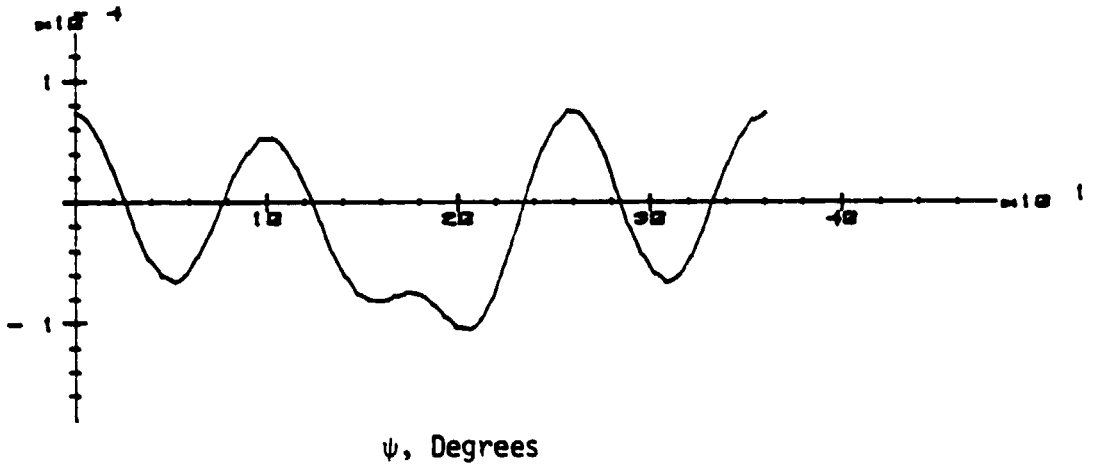

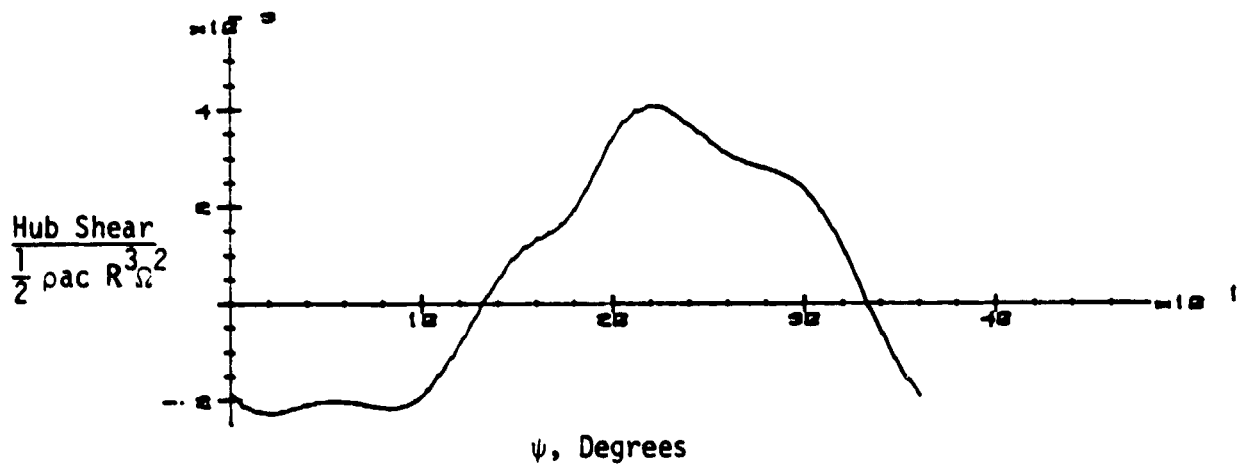

FIG. 5.1 Blade Response to Fuselage, Alone (No Pitch Control)

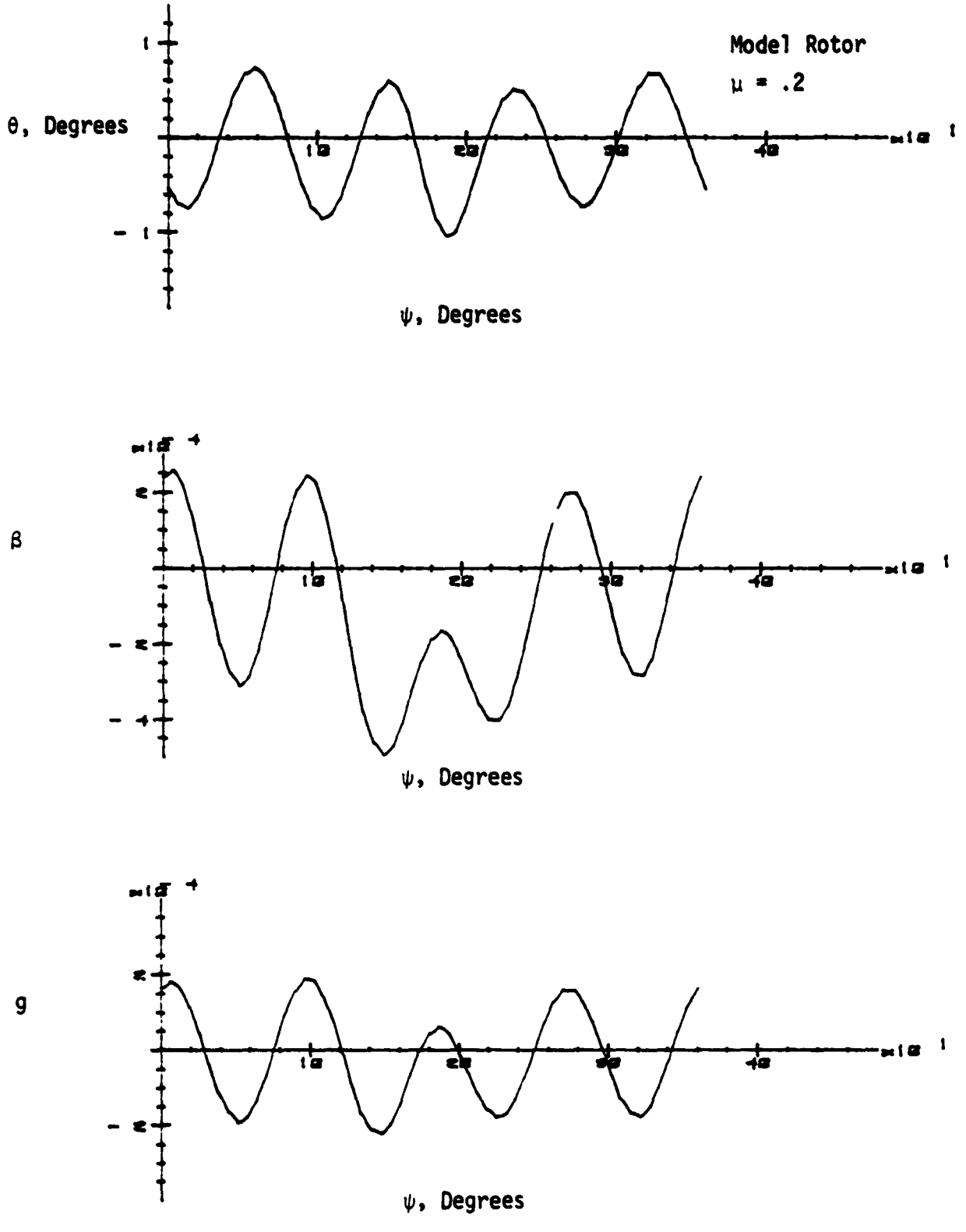

FIG. 5.2 Pitch Control for Zero Hub Shear; Resulting Blade Response

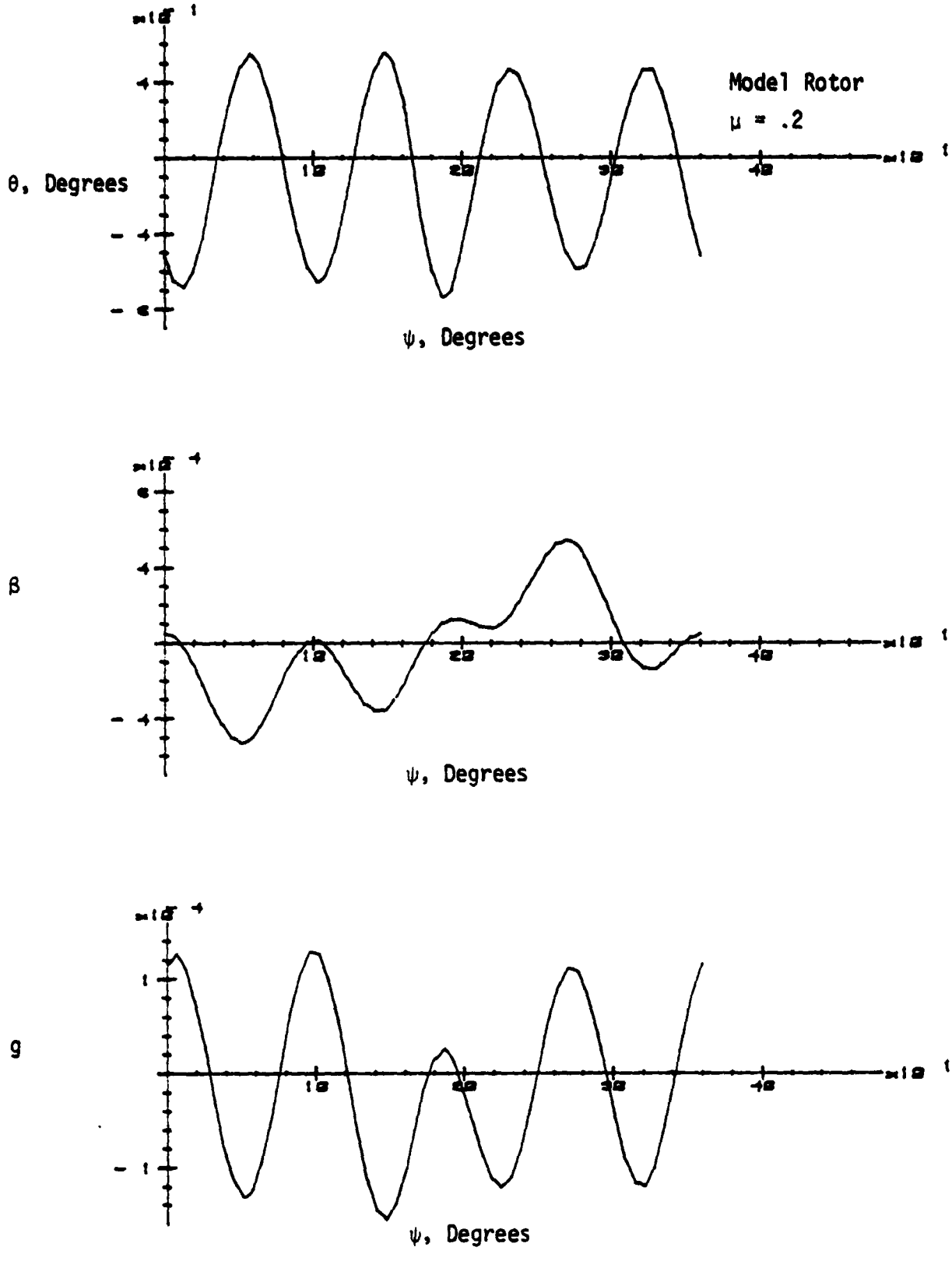

FIG. 5.3 Pitch Control for 80% Reduced Hub Shear; Resulting Blade Response

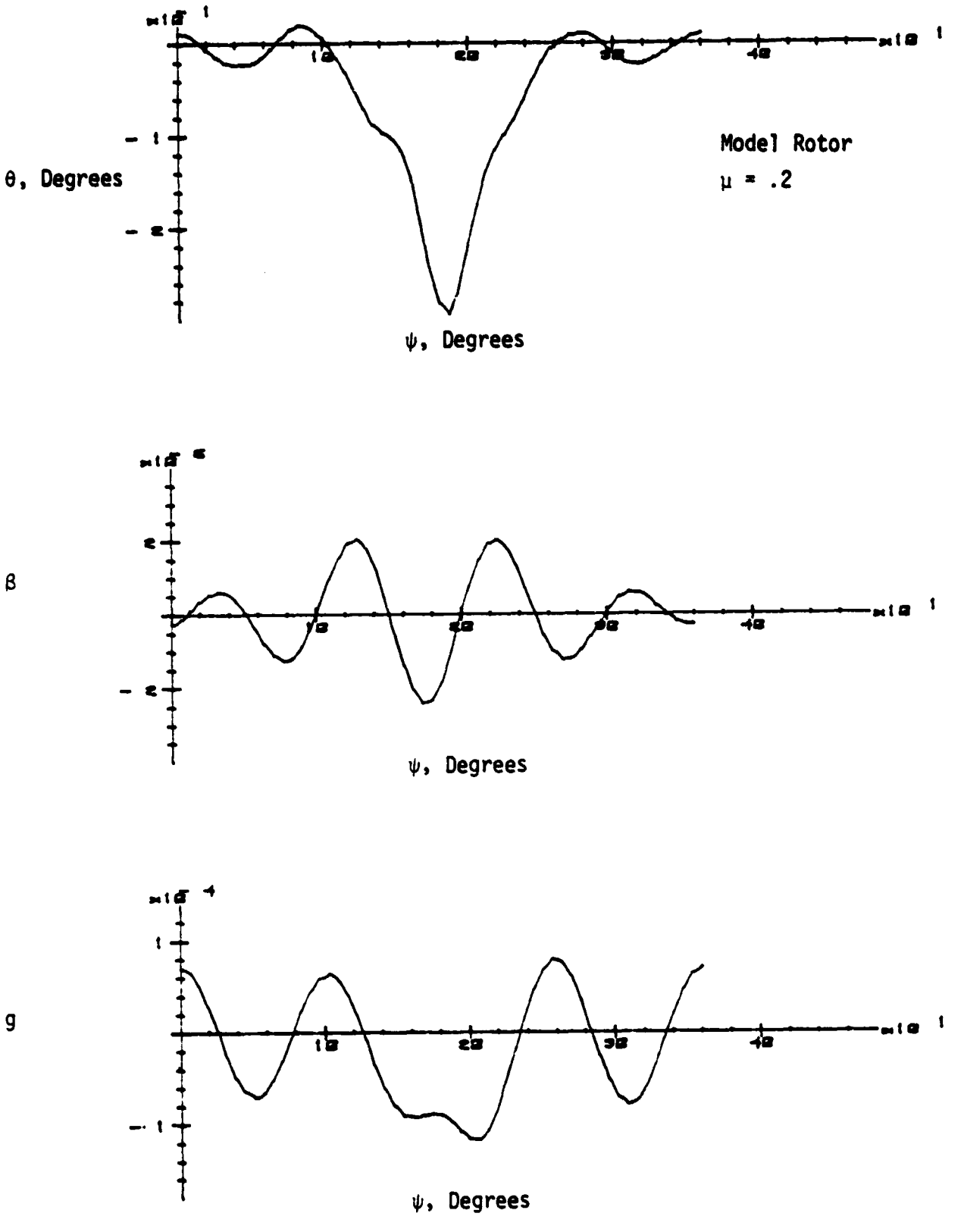

FIG. 5.4 Pitch Control for Minimum Blade Deflection; Resulting Blade Response

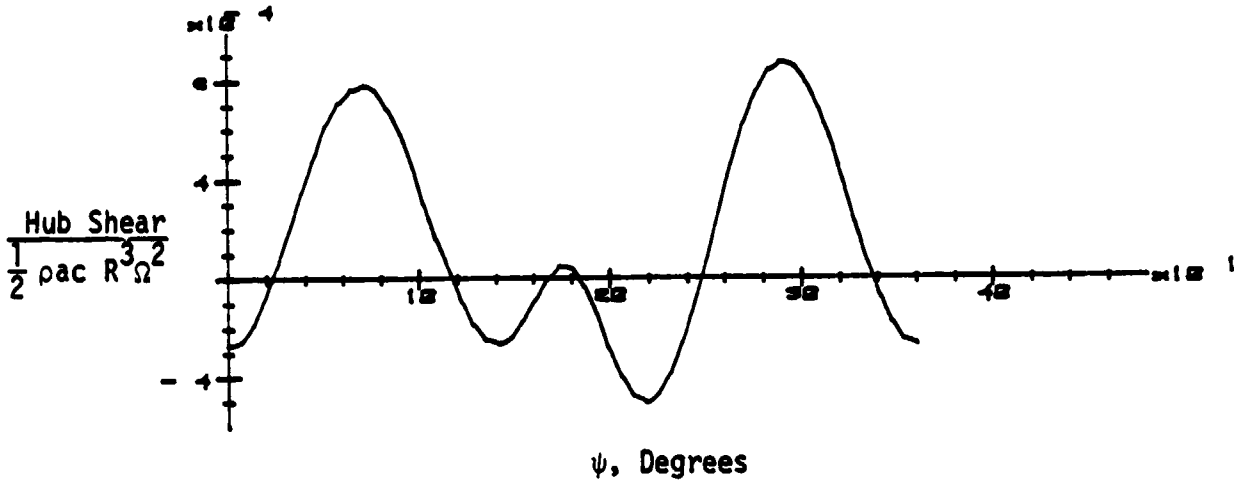

FIG. 5.4 Concluded

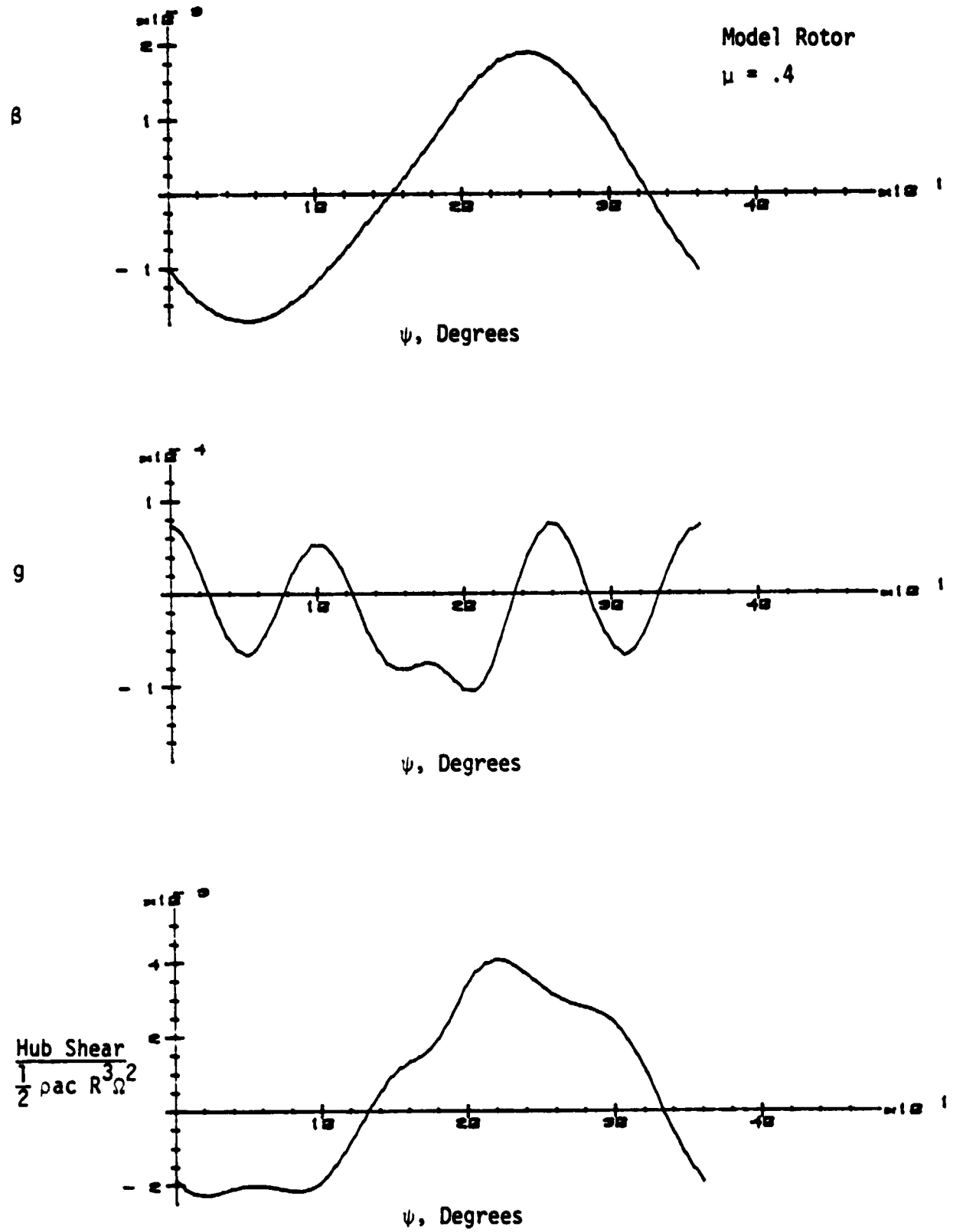

FIG. 5.5 Blade Response to Fuselage Alone (No Pitch Control)

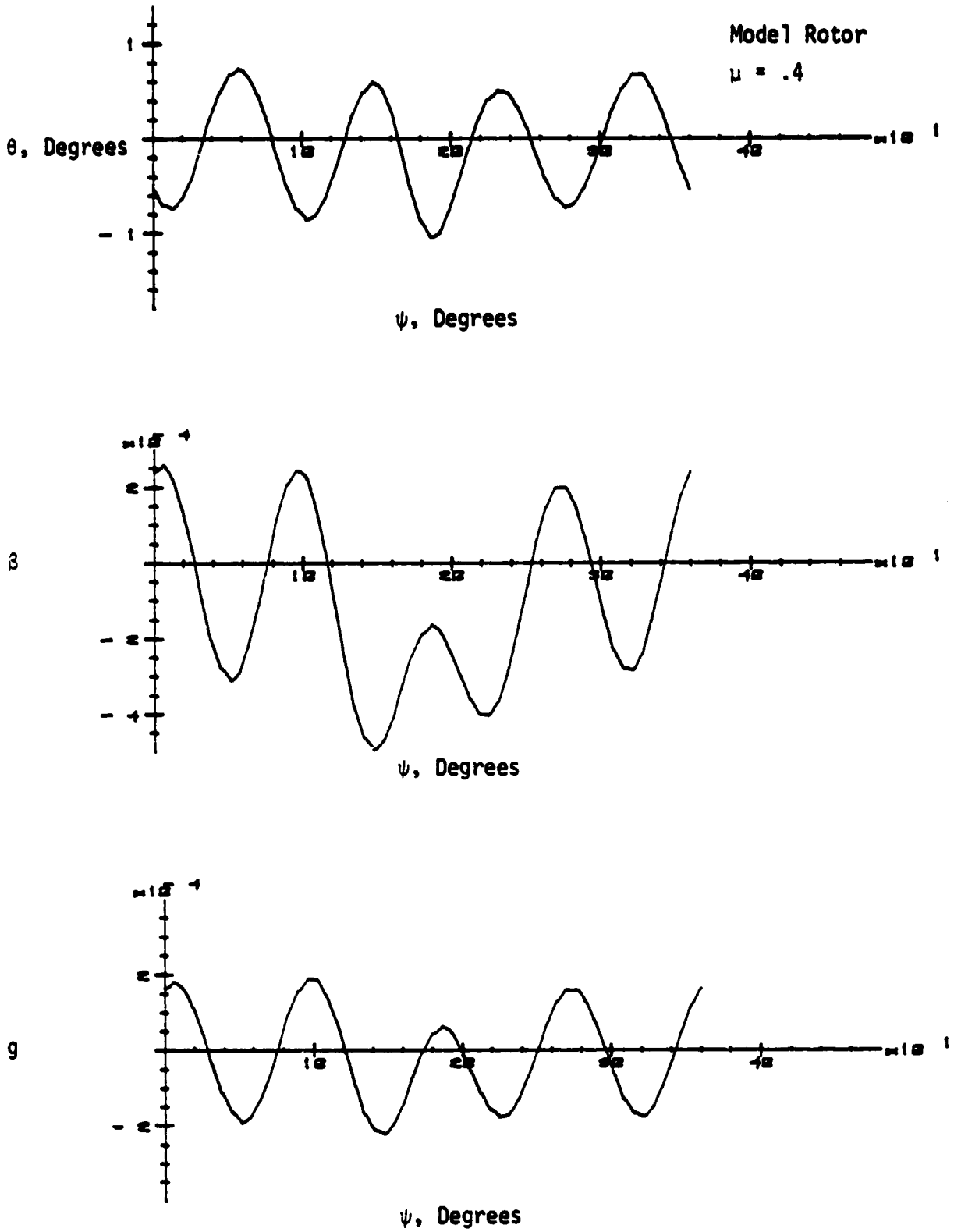

FIG. 5.6 Pitch Control for Zero Hub Shear; Resulting Blade Response

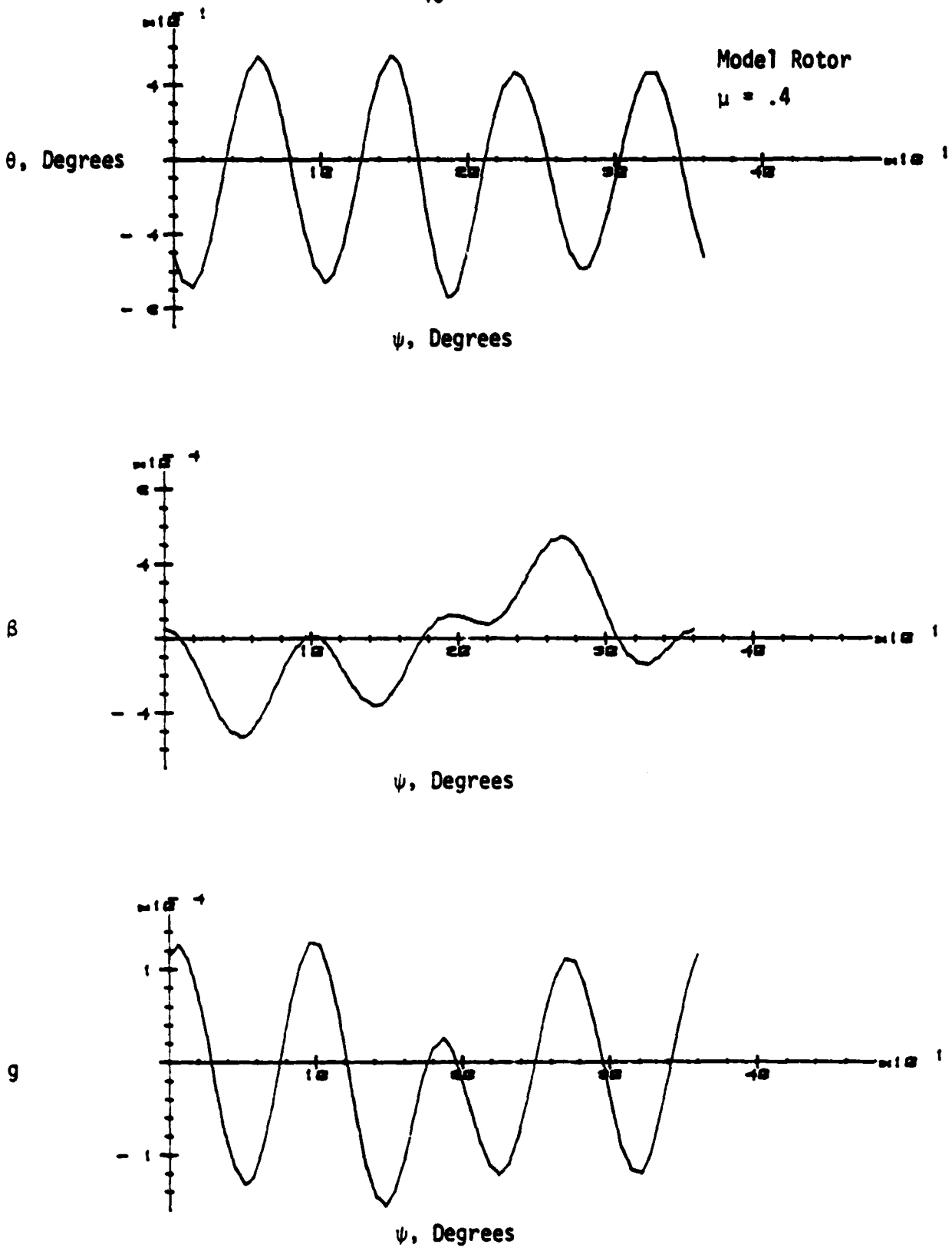

FIG. 5.7 Pitch Control for 80% Reduced Hub Shear; Resulting Blade Response

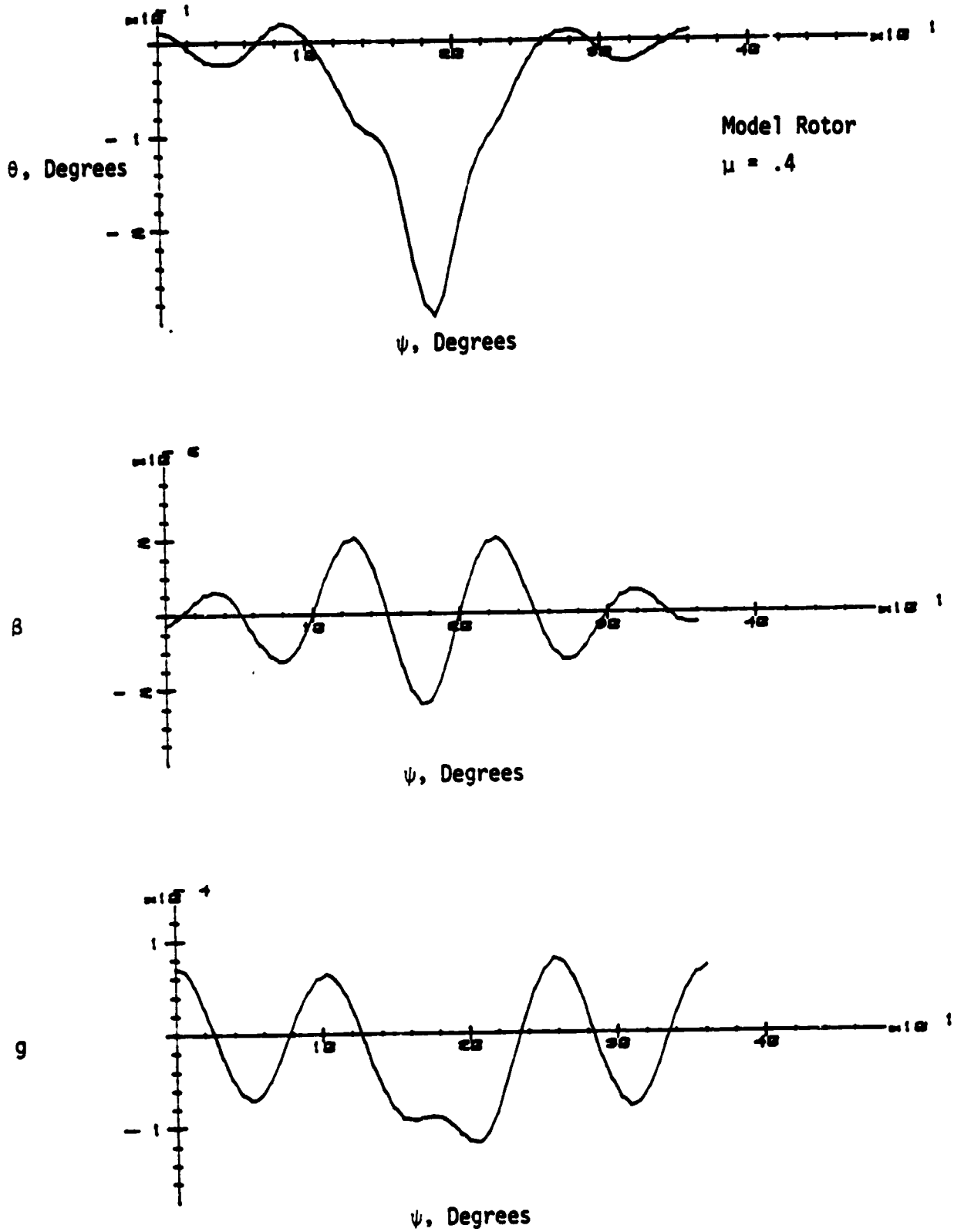

FIG. 5.8 PITCH CONTROL FOR MINIMUM Blade Deflection; Resulting Blade Response

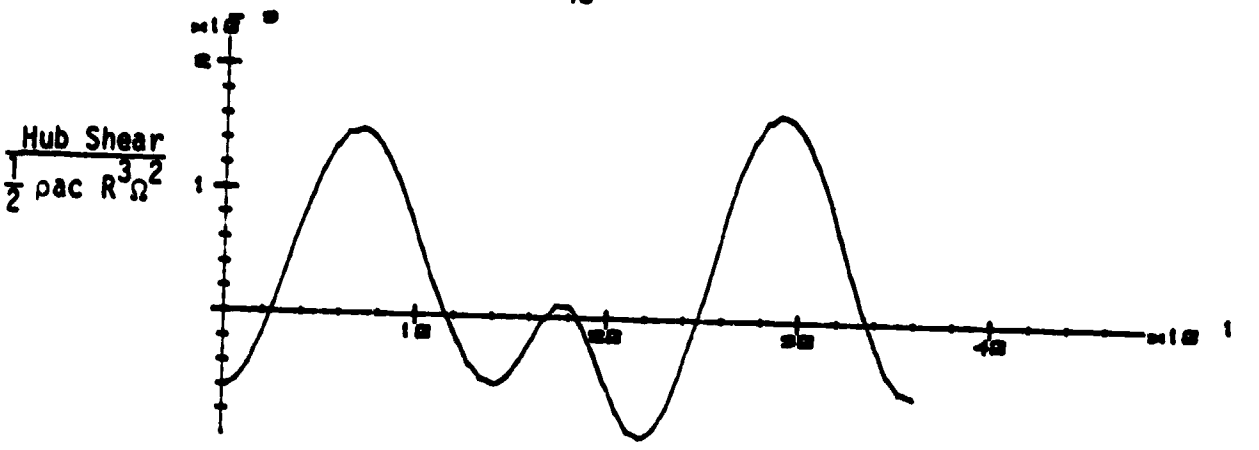

FIG. 5.8 Concluded

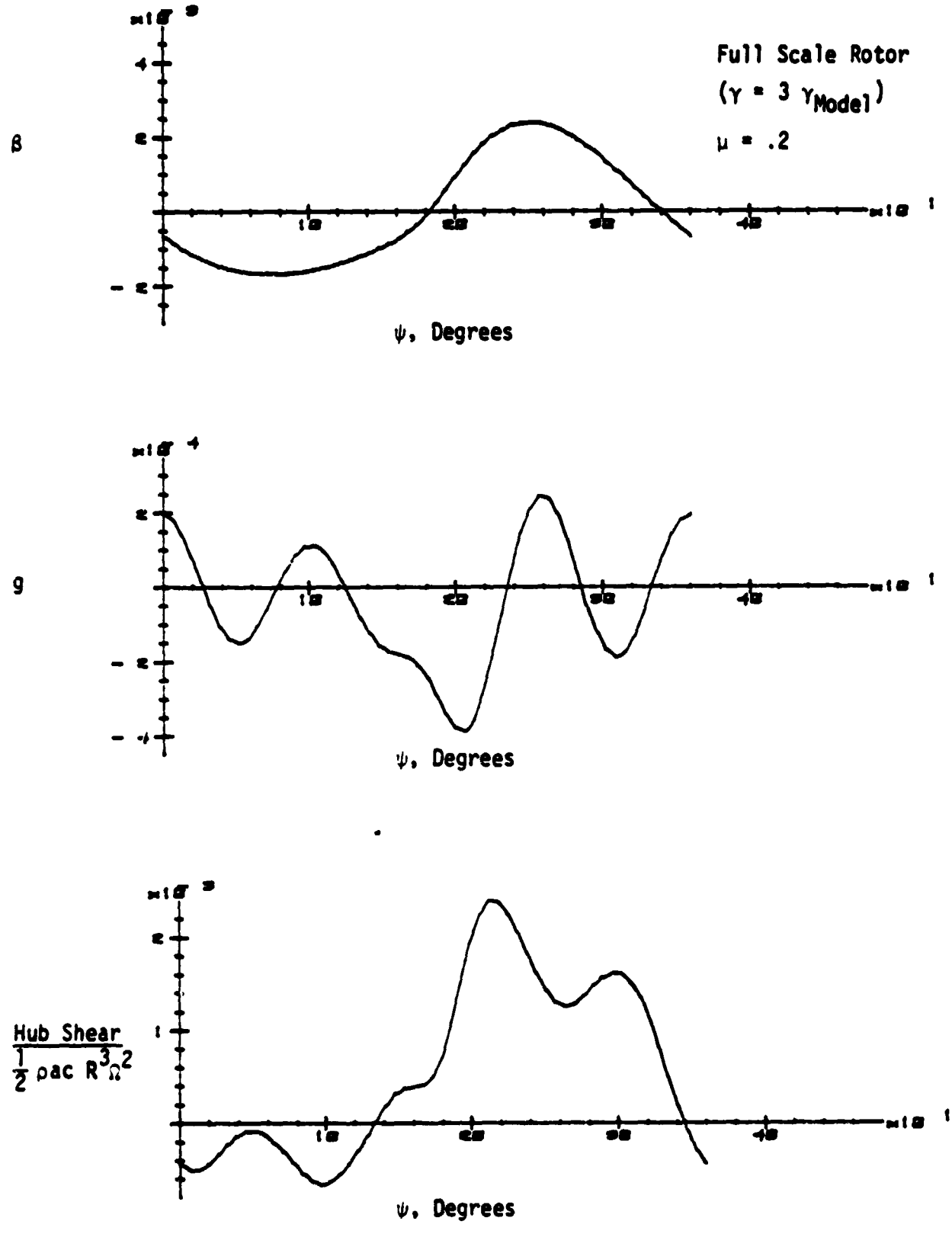

FIG. 5.9 Blade Response to Fuselage, Alone (No Pitch Control)

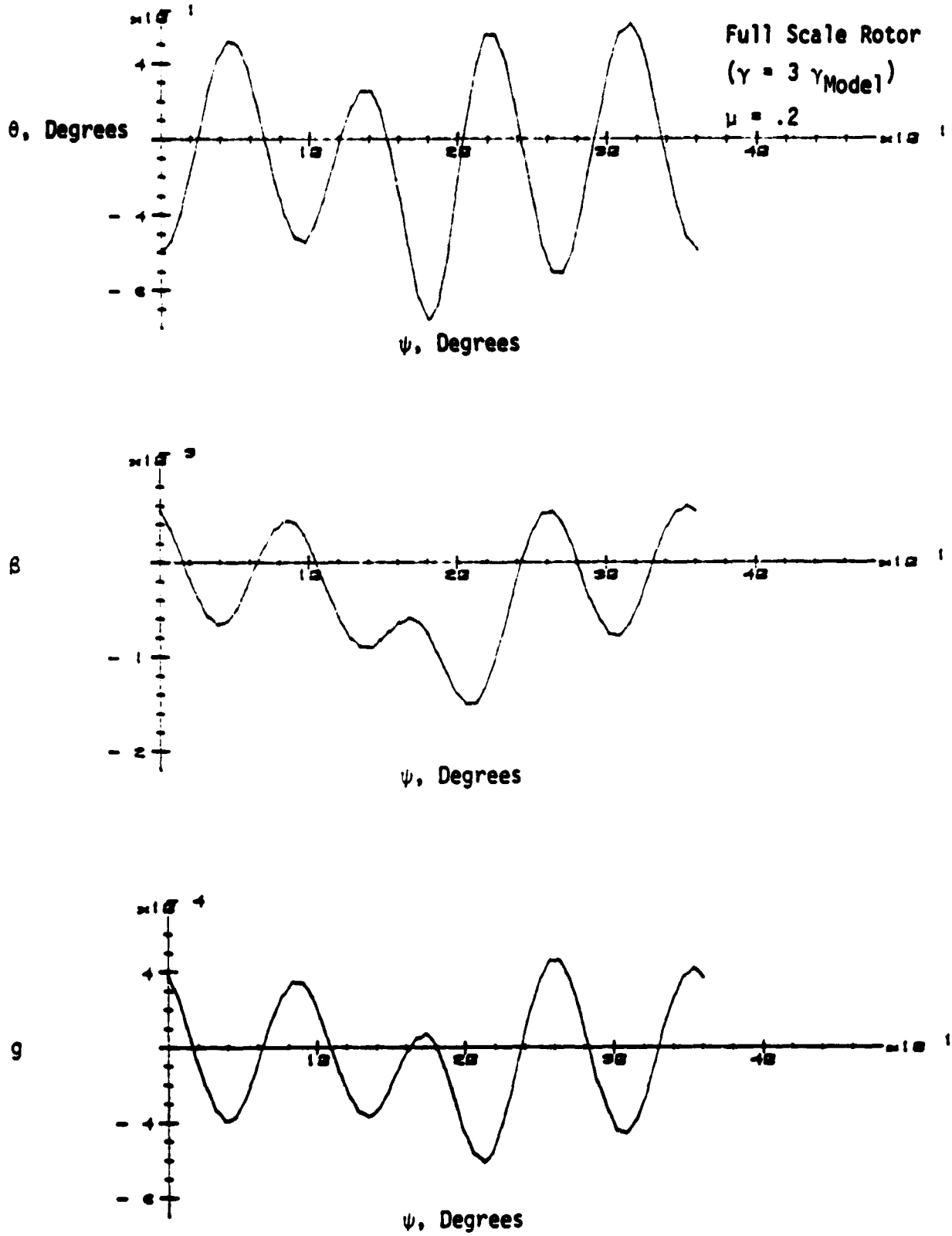

FIG. 5.10 Pitch Control for Zero Hub Shear; Resulting Blade Response

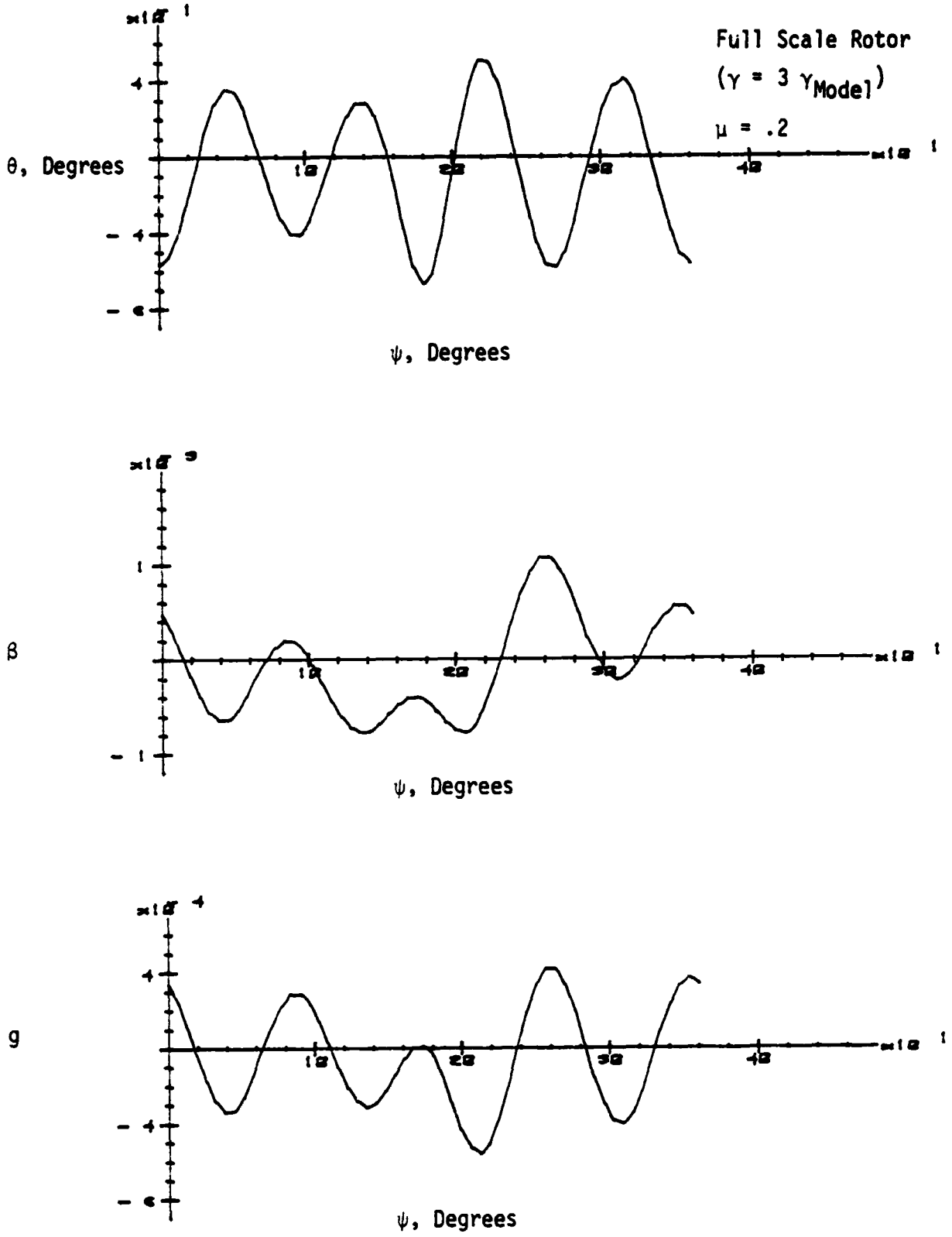

FIG. 5.11 Pitch Control for 80% Reduced Hub Shear; Resulting Blade Response

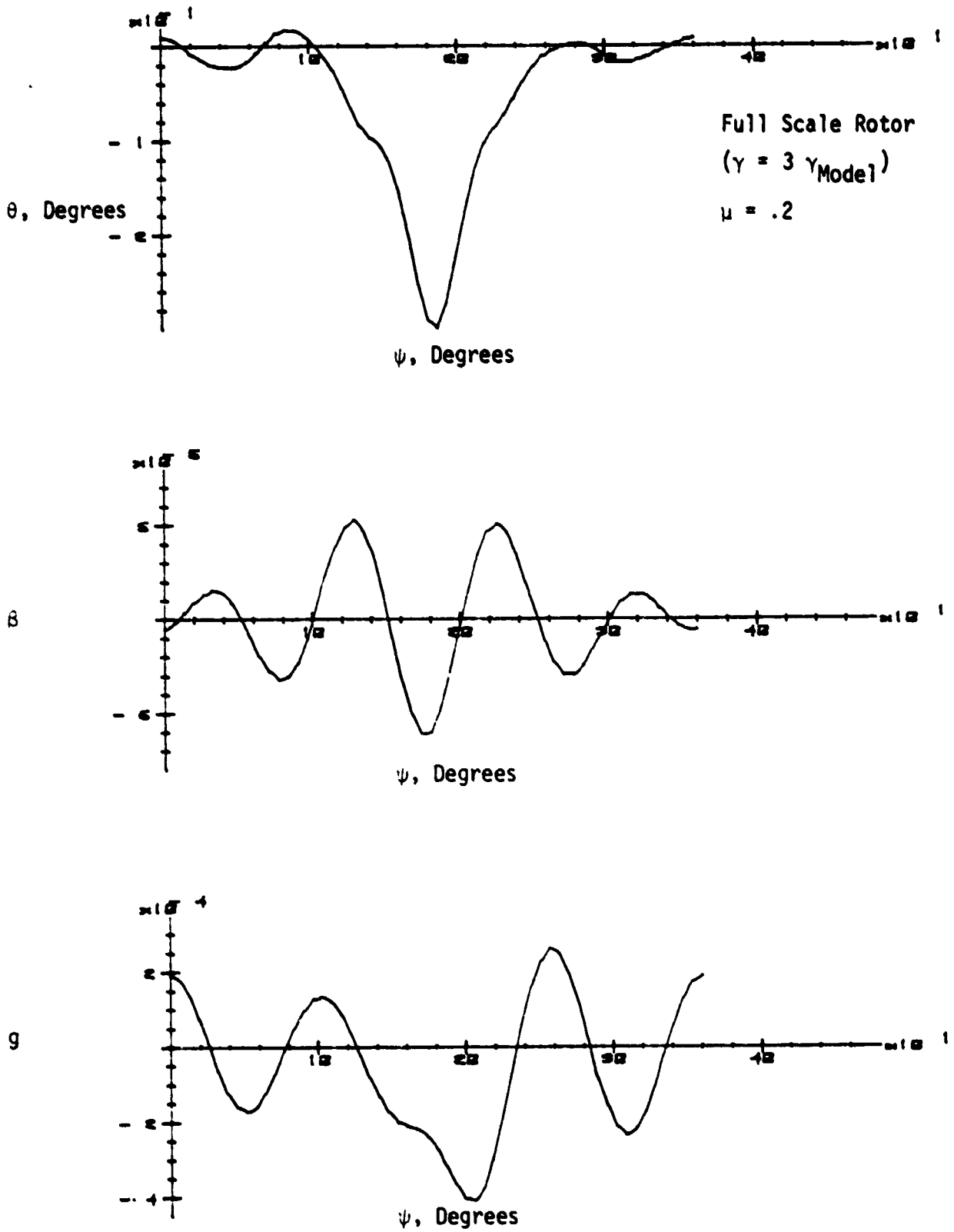

FIG. 5.12 Pitch Control for Minimum Blade Deflection; Resulting Blade Response

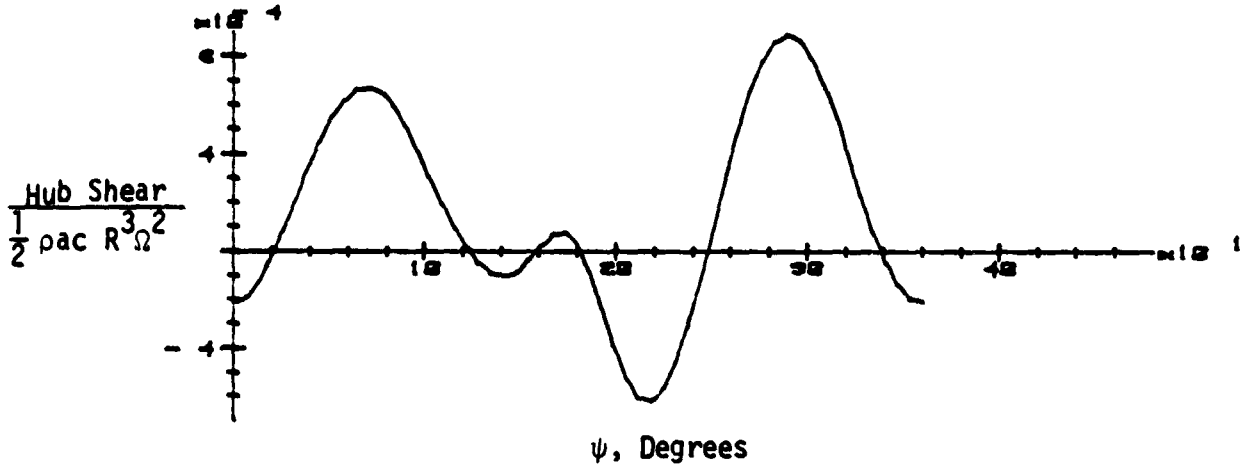

FIG. 5.12 Concluded

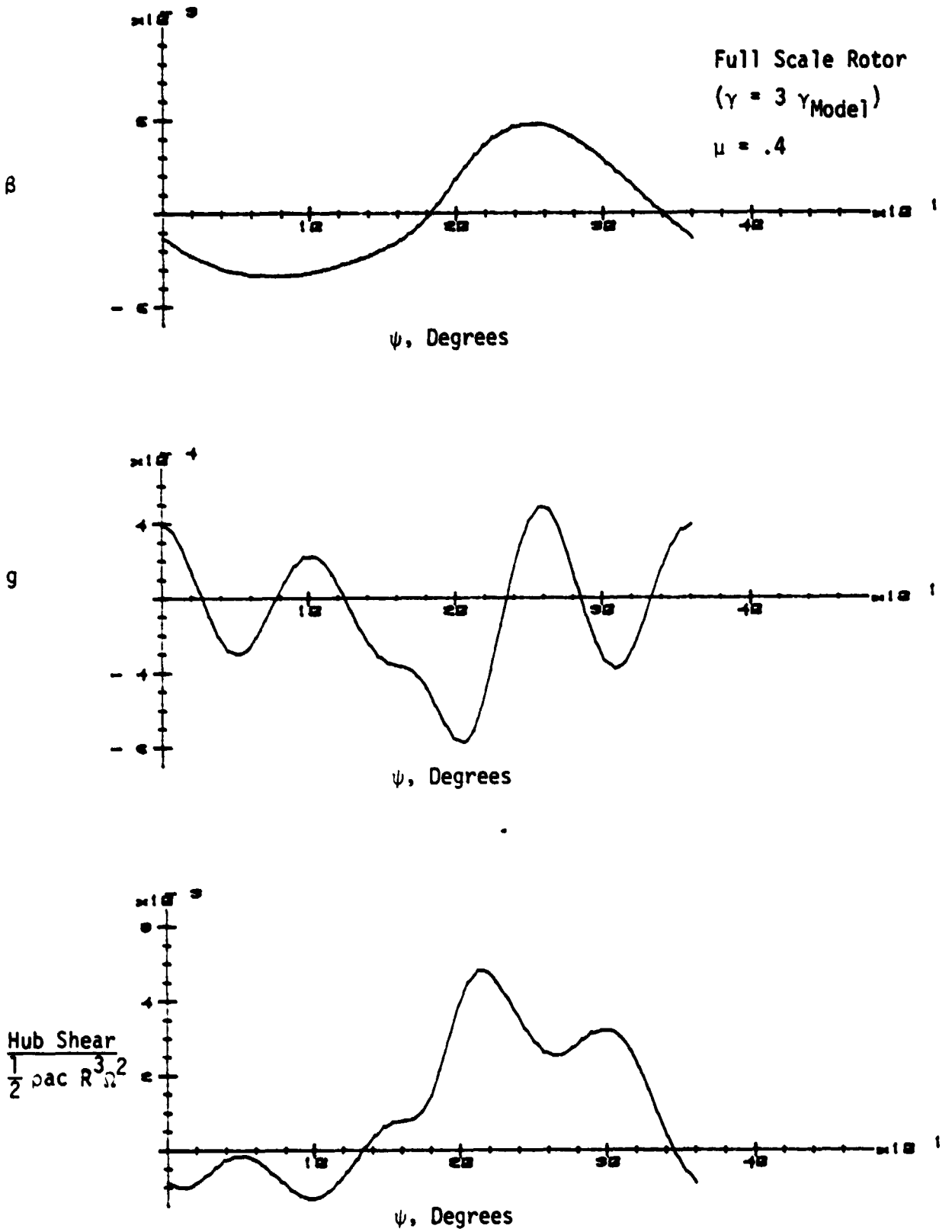

FIG. 5.13 Blade Response to Fuselage, Alone (No Pitch Control)

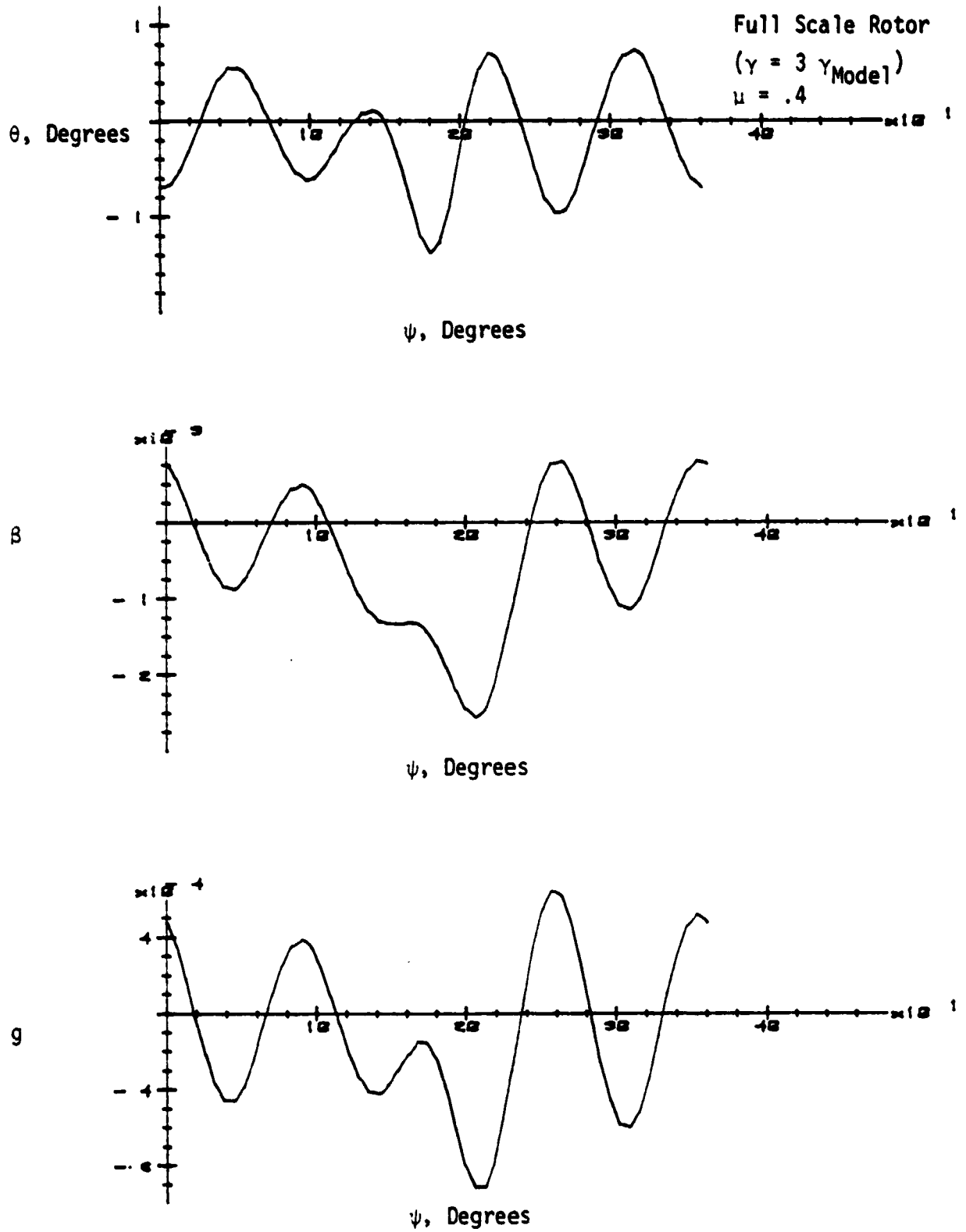

FIG. 5.14 Pitch Control for Zero Hub Shear; Resulting Blade Response

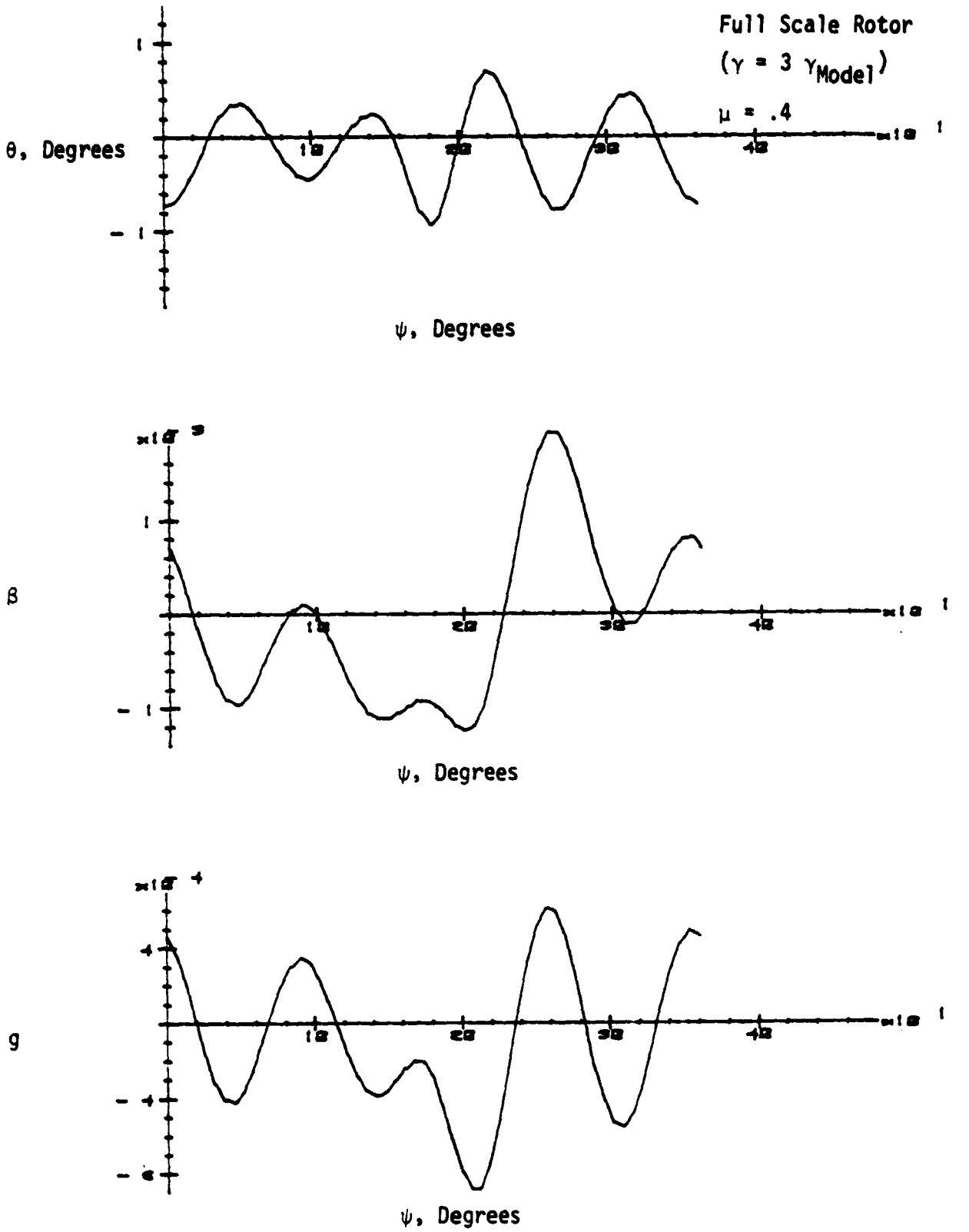

FIG. 5.15 Pitch Control for 80% Reduced Hub Shear; Resulting Blade Response

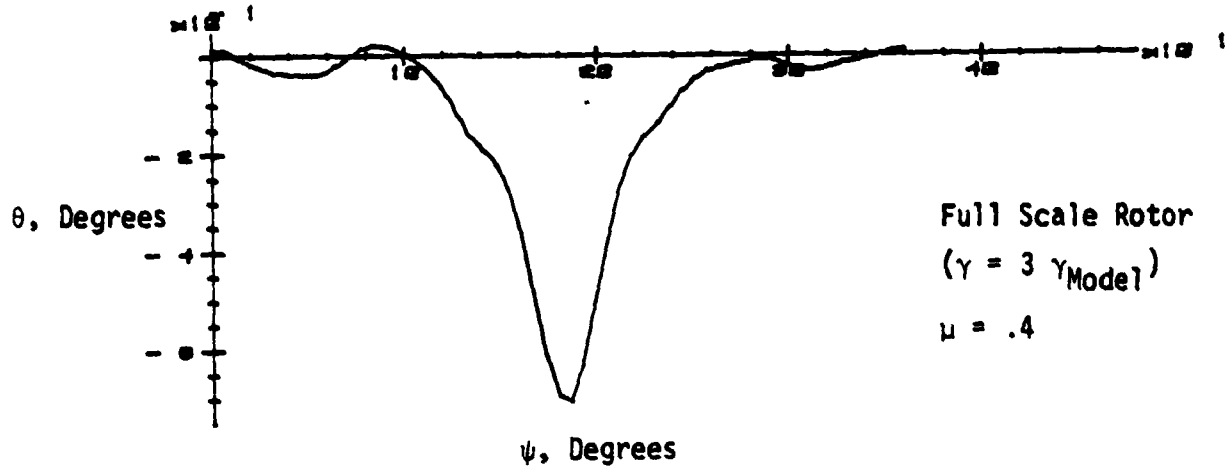

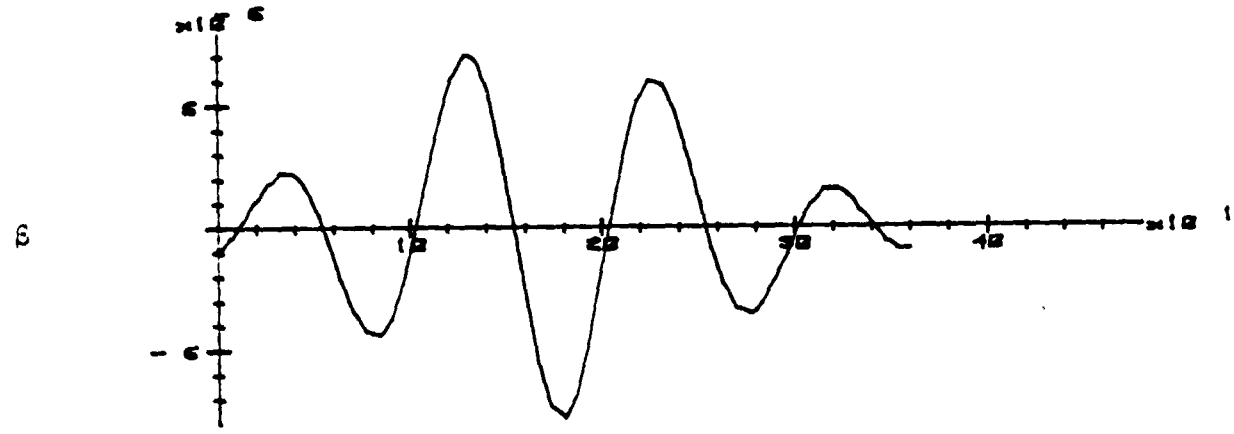

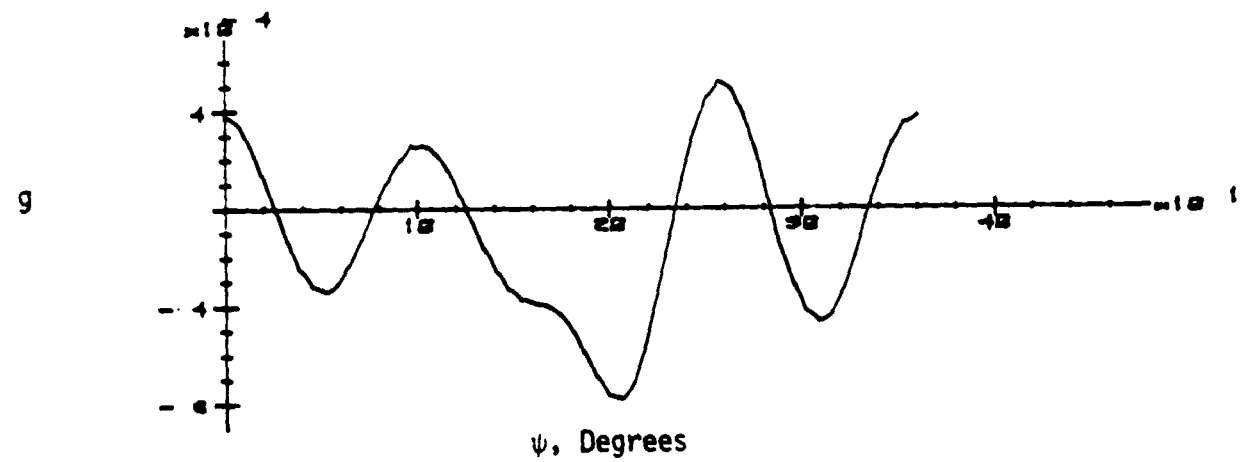

FIG. 5.16 Pitch Control for Minimum Blade Deflection; Resulting Blade Response

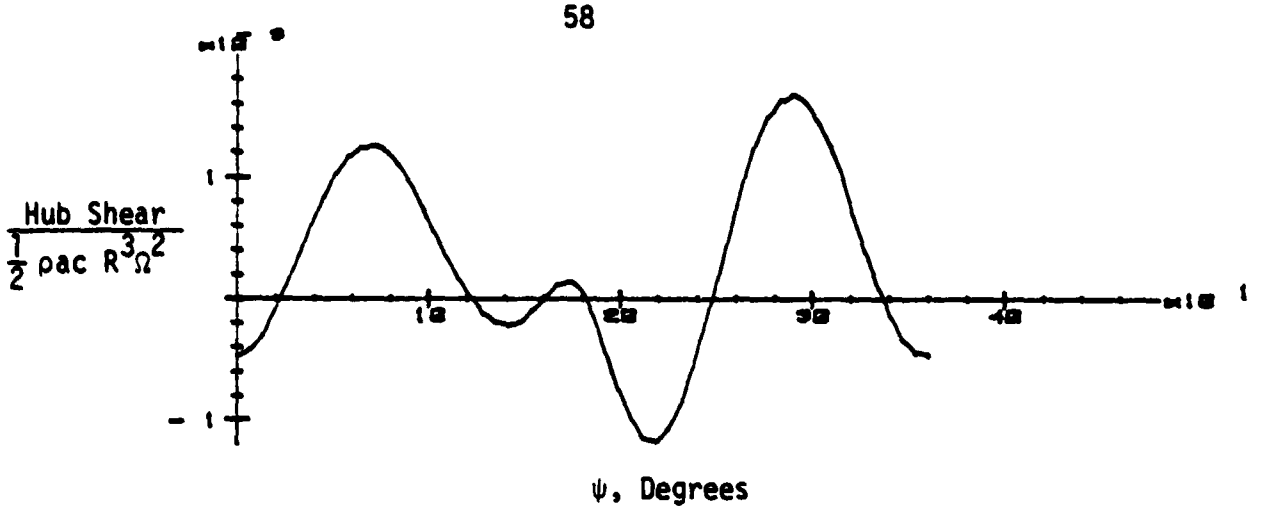

FIG. 5.16 Concluded

APPENDIX A

The general time dependent form of the various coefficients involved in the modal dynamic Equations (3.9a,b) are:

$$m_{\beta_1'} = \frac{\gamma}{2}\bar{C}'(K)\int_{\xi}^{1}(x+\mu\sin\psi)\frac{n_1^2}{R^2}\,dx$$

$$m_{g_1'} = \frac{\gamma}{2}\bar{C}'(K)\int_{\xi}^{1}(x+\mu\sin\psi)\left(\frac{n_1}{R}\right)\left(\frac{n_2}{R}\right)dx$$

$$m_{\beta_1} = r_1^2 + \frac{\gamma\bar{C}'(K)}{2}\int_{\xi}^{1}(x+\mu\sin\psi)\mu\cos\psi\cdot\left(\frac{n_1}{R}\right)\frac{d}{dx}\left(\frac{n_1}{R}\right)dx$$

$$m_{g_1} = \frac{\gamma\bar{C}'(K)}{2}\int_{\xi}^{1}(x+\mu\sin\psi)\mu\cos\psi\cdot\left(\frac{n_1}{R}\right)\frac{d}{dx}\left(\frac{n_2}{R}\right)dx$$

$$m_{\theta_1'} = \frac{1}{2}\gamma(cR)\left[\bar{C}'(K)\cdot\left(.5-\frac{x_A}{c}\right)+\frac{1}{4}\right]\int_{\xi}^{1}\left(x+\mu\sin\psi\right)\frac{n_1}{R}\,dx$$

$$m_{\theta_1} = \frac{\gamma\bar{C}'(K)}{2}\int_{\xi}^{1}\left(x+\mu\sin\psi\right)^2\frac{n_1}{R}\,dx$$

$$m_{\beta_2'} = \frac{\gamma(RM)\bar{C}'(K)}{2}\int_{\xi}^{1}(x+\mu\sin\psi)\frac{n_1}{R}\cdot\frac{n_2}{R}\,dx$$

$$m_{g_2'} = \frac{\gamma(RM)\bar{C}'(K)}{2}\int_{\xi}^{1}(x+\mu\sin\psi)\left(\frac{n_2}{R}\right)^2dx$$

$$m_{\beta_2} = \frac{\gamma(RM)\bar{C}'(K)}{2}\int_{\xi}^{1}(x+\mu\sin\psi)\mu\cos\psi\cdot\left(\frac{n_2}{R}\right)\frac{d}{dx}\left(\frac{n_1}{R}\right)dx$$

$$m_{\beta_2} = \nu_2^2 + \frac{\gamma(RM)\bar{C}'(K)}{2}\int_{\xi}^{1}(x+\mu\sin\psi)\mu\cos\psi\cdot\left(\frac{n_2}{R}\right)\frac{d}{dx}\left(\frac{n_2}{R}\right)dx$$

$$m'_{\theta_2} = \frac{1}{2}\gamma(RM)(CR)\left[\bar{C}'(K)\cdot\left(.5-\frac{x_A}{c}\right)+\frac{1}{4}\right]\int_{\xi}^{1}(x+\mu\sin\psi)\frac{n_2}{R}dx$$

$$m_{\theta_2} = \frac{\gamma(RM)\bar{C}'(K)}{2}\int_{\xi}^{1}(x+\mu\sin\psi)^2\frac{n_2}{R}dx$$

where γ is the Lock number defined as

$$\gamma \equiv \frac{\rho a c R^4}{M_1}$$

RM is the ratio M_1/M_2 given in Eq. (3.11)

$\overline{C'(K)}$ is representative of a mean value for $C'(K)$ over the blade span, usually based on conditions at blade three-quarter radius. For quasi-steady air flor, $\overline{C'(K)} = 1$.

The time (ψ) averaged coefficients expressed in Eq. (3.10) were calculated from the above relations using a value of (.0821) for the hinge offset (ξ), 0 for X_A and quasi-steady air flow was assumed ($C'(K) = 1$).

APPENDIX B

Fuselage Aerodynamic Forcing Functions

The expressions for the forcing functions $F_{\lambda_1}(\psi)$ and $F_{\lambda_2}(\psi)$ representing the upwash flow effect of the fuselage in Eqs. (3.9a,b) are:

$$F_{\lambda_1}(\psi) = \frac{\mu \gamma \bar{c}'(K)}{2} \int_{\xi}^{1} (x + \mu \sin\psi) \frac{n_1}{R} \cdot \lambda(x,\psi)\, dx \tag{B.1}$$

$$F_{\lambda_2}(\psi) = \frac{\mu \gamma (RM)\, \bar{c}'(K)}{2} \int_{\xi}^{1} (x + \mu \sin\psi) \frac{n_2}{R} \cdot \lambda(x,\psi)\, dx$$

where $\lambda(x,\psi)$ is the fuselage upwash given in Eq. (2.2), which is of the form

$$\lambda(x,\psi) = \frac{H}{16\left[Cx^2 - Bx\cos(\pi-\psi) + A\right]^{3/2}} \tag{B.2}$$

Now, the terms involving sin ψ in Eq. (b.1) are averaged to zero in time because of the symmetric property of $\lambda(\psi,n)$ about $\psi = \pi$. Besides, they are also expected to be small compared to the remaining terms, considering that $\lambda(n,\psi)$ is concentrated around 180° azimuth (where sin ψ is small) as is noticed from Figure (2.3).

The forcing functions are then approximated in time averaged form to:

$$F_{\lambda_1}(\psi) \simeq \frac{\mu\gamma\bar{c}'(k)}{2}\int_{\xi}^{1} x\left(\frac{n_1}{R}\right) h(x,\psi)\,dx$$

$$F_{\lambda_2}(\psi) \simeq \frac{\mu\gamma(RM)\bar{c}'(k)}{2}\int_{\xi}^{1} x\left(\frac{n_2}{R}\right) h(x,\psi)\,dx \qquad \text{(B.3)}$$

The functions n_1 and n_2 are the rigid flap and 1st bending mode.

$$\frac{n_1}{R} = \frac{x-\xi}{1-\xi}$$

$$\frac{n_2}{R} \doteq 4\left(\frac{x-\xi}{1-\xi}\right)^2 - 3\left(\frac{x-\xi}{1-\xi}\right)$$

with these and the expression for $\lambda(n,\psi)$ given in Eq. (B.2), Eqs. (B.3) in integrated form become

$$F_{\lambda_1}(\psi) = \frac{\mu\gamma\bar{c}'(k)}{2}\left[F(1,\psi) - F(\xi,\psi)\right]$$

$$F_{\lambda_2}(\psi) = \frac{\mu\gamma(RM)\bar{c}'(k)}{2}\left[G(1,\psi) - G(\xi,\psi)\right]$$

in which $F(x,\psi)$ and $G(x,\psi)$ denote the following expressions:

$$F(x, \cdot \quad \frac{H}{16(1-\xi)}\left\{U(x,\psi)\cdot\left(\xi - \frac{B}{2C}\cos(\pi-\psi)\right) + \right.$$

$$+\frac{1}{c\sqrt{c}}\sinh^{-1}\frac{2cx-B\cos(n-\psi)}{\sqrt{4AC-B^2\cos^2(n-\psi)}}-\frac{x}{c\sqrt{cx^2-Bx\cos(n-\psi)+A}}\Bigg\}$$

$$G(x,\psi)=\frac{H}{4(1-\varepsilon)^2}\Bigg\{\frac{1}{c\sqrt{cx^2-Bx\cos(n-\psi)+A}}\left(x^2-\frac{3B}{2C}x\cdot\cos(n-\psi)\right)$$

$$+U(x,\psi)\cdot\left(\frac{8AC-3B^2\cos^2(n-\psi)}{4C^2}+\frac{\varepsilon B}{C}\cos(n-\psi)-\varepsilon^2\right)$$

$$+\frac{2\varepsilon\cdot x}{c\sqrt{cx^2-Bx\cos(n-\psi)+A}}+\frac{1}{c\sqrt{c}}\left(-2\varepsilon+\frac{3B}{2C}\cos(n-\psi)\right)\cdot$$

$$\sinh^{-1}\frac{2cx-B\cos(n-\psi)}{\sqrt{4AC-B^2\cos^2(n-\psi)}}\Bigg\}-3F(x,\psi)$$

in which

$$U(x,\psi)\equiv\frac{1}{c\sqrt{cx^2-Bx\cos(n-\psi)+A}}\left(1-\frac{B(2cx-B\cos(n-\psi))}{4AC-B^2\cos^2(n-\psi)}\cos(n-\psi)\right)$$

The integral denoted by $T(\psi)$ in the expression for blade hub shear of Chapter 4, is integrated to

$$T(\psi)\equiv\int_{\varepsilon}^{1}x\,\lambda(x,\psi)\,dx=\frac{-2H\left(2A-Bx\cos(n-\psi)\right)}{16\left[4AC-B^2\cos^2(n-\psi)\right]\sqrt{cx^2-Bx\cos(n-\psi)+A}}\Bigg|_{\varepsilon}^{1}$$

The parameters H, A, B and C involved in λ (Eq. B.2) are related to the orientation of rotor with respect to the fuselage. The values used in the numerical calculations are from Eq. (2.2a):

$$H = .79$$

$$C = 16.52$$

$$B = 16.86$$

$$A = 4.92$$

The harmonic components of the functions F, G and T were calculated using the numerical procedure for the Fourier analysis outlined in [8]. The Fourier expansions thus obtained were plotted together with corresponding exact functions, in Figs. (B-1,3), using 9 harmonics. In the numerical calculations, nine harmonics were used to approximate each function.

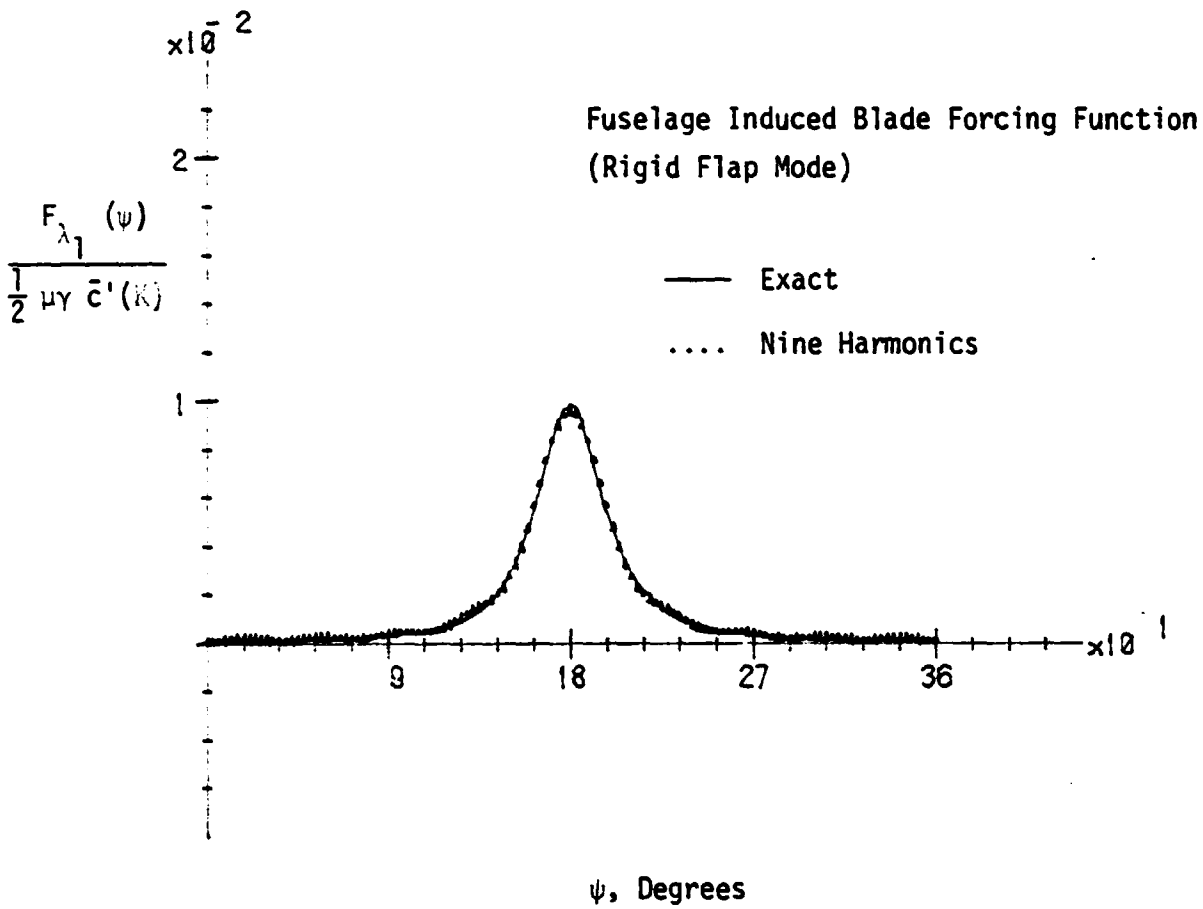
x10⁻²
2
1
$\frac{F_{\lambda_1}(\psi)}{\frac{1}{2}\mu\gamma\bar{c}'(K)}$
Fuselage Induced Blade Forcing Function
(Rigid Flap Mode)
—— Exact
.... Nine Harmonics
9
18
27
36
x10
1
ψ, Degrees

FIG. B.1

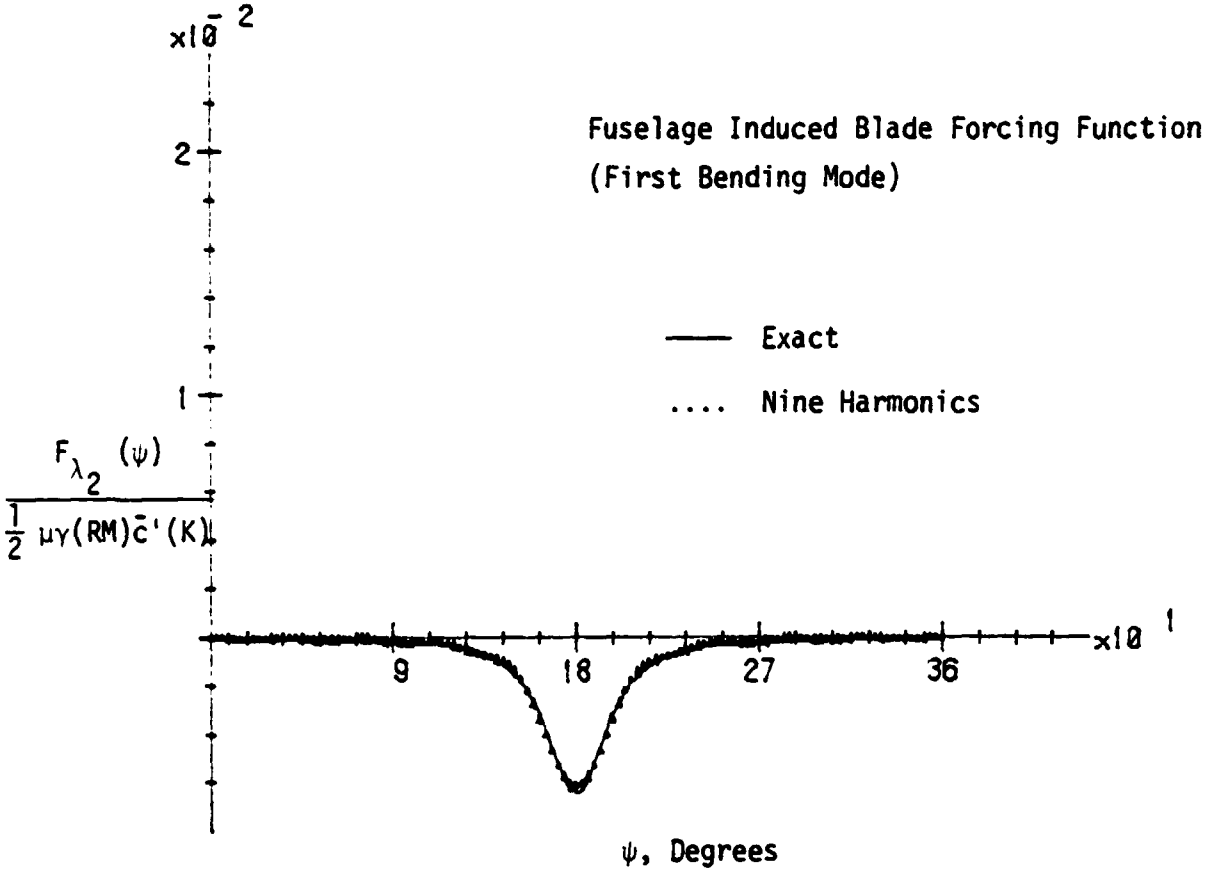
x10⁻²
2
1
$F_{\lambda_2}(\psi)$
$\frac{1}{2}\mu\gamma(RM)\bar{c}'(K)$
9
18
27
36
x10¹
Fuselage Induced Blade Forcing Function
(First Bending Mode)
—— Exact
.... Nine Harmonics
ψ, Degrees

FIG. B.2

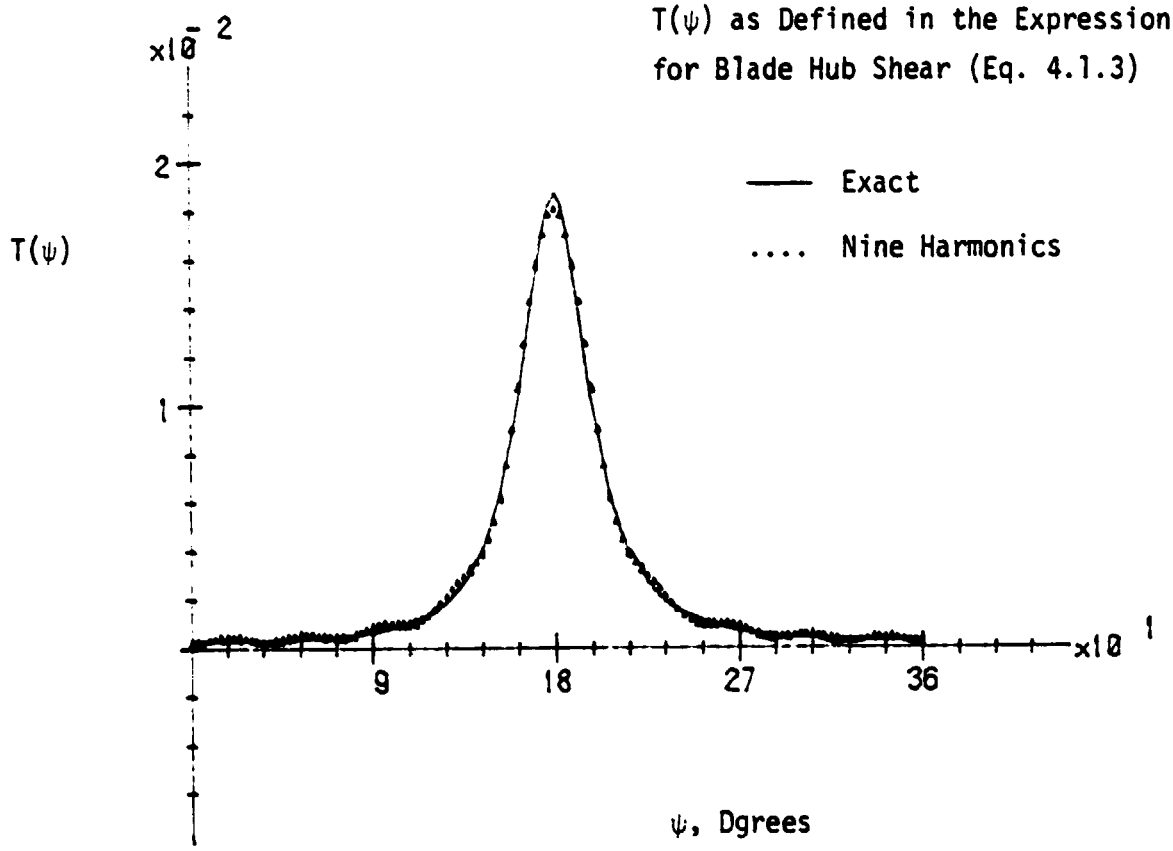
T(ψ) as Defined in the Expression
for Blade Hub Shear (Eq. 4.1.3)
Exact
Nine Harmonics
T(ψ)
x10 2
2
1
x10 1
9
18
27
36
ψ, Dgrees

FIG. B.3